

INVESTIGATION OF LASER DYNAMICS, MODULATION AND CONTROL
BY MEANS OF INTRA-CAVITY TIME VARYING PERTURBATION

under the direction of
S. E. Harris

Semiannual Status Report
(Report No. 22)

for

NASA Grant NGL-05-020-103

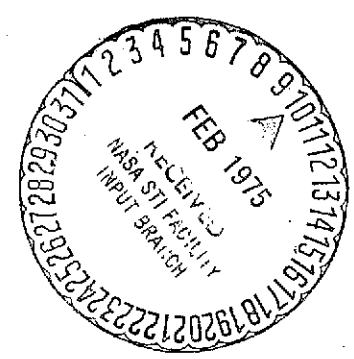
National Aeronautics and Space Administration
Washington, D.C.

for the period

1 August 1974 - 31 January 1975

M. L. Report No. 2404

February 1975



Microwave Laboratory
W. W. Hansen Laboratories of Physics
Stanford University
Stanford, California

(NASA-CR-142018) INVESTIGATION OF LASER DYNAMICS, MODULATION AND CONTROL BY MEANS OF INTRA-CAVITY TIME VARYING PERTURBATION Semiannual Status Report, 1 Aug. 1974 - 31 Jan. 1975 (Stanford Univ.) 77 p HC \$4.25 N75-15971 Unclas G3/36 07766

STAFF

NASA Grant NGL-05-020-103

for the period

1 August 1974 - 31 January 1975

PRINCIPAL INVESTIGATOR

S. E. Harris

PROFESSOR

A. E. Siegman

RESEARCH ASSOCIATES

D. J. Kuizenga

A. H. Kung

J. F. Young

RESEARCH ASSISTANTS

G. W. Bekkers

D. M. Bloom

J. H. Newton

D. W. Phillion

I. INTRODUCTION

The general goal of this grant is to undertake research on the generation of tunable visible, infrared, and ultraviolet light, and on the control of this light by means of novel mode-locking and modulation techniques. During this reporting period the following projects have been active: (1) transient mode-locking of the Nd:YAG laser and generation of short tunable pulses in the visible; (2) investigations of the alkali metal inert gas excimer laser systems; (3) techniques for frequency conversion of high power and high energy laser radiation; and (4) high average power blue and UV laser light sources. These projects are described in detail in Section II of this report. Although the coherent vacuum ultraviolet holography project is currently inactive, a paper based on that work has been submitted for publication. It is entitled "Effects of Focusing on Third Order Non-linear Processes in Isotropic Media" by G. C. Bjorklund and is attached as Appendix A.

II. SUMMARY OF PROGRESS

A. Transient Mode-Locking of the Nd:YAG Laser, and Generation of Short, Tunable Pulses in the Visible

(D. W. Phillion,^{*} D. J. Kuizenga, and A. E. Siegman)

For the past several report periods this project has been concerned with the theoretical understanding and experimental optimization of short-pulse generation in Nd:YAG lasers when these lasers are continuously pumped, repetitively Q-switched, and simultaneously mode-locked.^{1,2} During the past period this work has led to the completion of a Nd:YAG laser that generates a continuous train of single mode-locked pulses at a repetition rate of 500 single pulses per second, each pulse having a peak power of 0.5 - 1.0 MW and a pulsewidth of ~ 60 psec. The technique of "pre-lasing" developed under this contract is used to overcome the transient build-up problem for mode-locking of the laser, so as to achieve this pulsewidth. A single pulse is selected from each burst of repetitively Q-switched and mode-locked laser output by means of a z-cut LiNbO_3 electro-optic switch. The kilovolt level, nanosecond rise time pulse that activates this switch is synchronized to the pulse burst by a fast photodiode, fast logic circuitry, and an avalanche transistor chain for generating the pulse.

^{*} Ph.D. dissertation completed, now at Lawrence Livermore Laboratories.

The resulting train of $1.064 \mu\text{m}$ pulses can then be doubled to 532 nm with $> 35\%$ conversion efficiency in an elliptically focused LiIO_3 crystal; and we are presently working on further doubling of the pulses to 266 nm in a CDA crystal.

This laser has a peak power ($10^5 - 10^6 \text{ W}$) much closer to a flash-pumped mode-locked YAG laser ($10^7 - 10^9 \text{ W}$) than to a cw-pumped mode-locked YAG laser ($10^1 - 10^2 \text{ W}$), at a substantially higher repetition rate than in a flash-pumped laser. Yet it has essentially the same stability, spectral purity and reproducibility as does a cw mode-locked laser. Hence it will be ideally suited as a high-repetition-rate source for many short-pulse applications, including as a master oscillator for lunar ranging experiments; for airborne optical radar profiling of water turbidity; for non-linear optics experiments; and for basic physical measurements of fast atomic and molecular relaxation processes, an area we are presently pursuing.

The pulsewidth of this laser is, however, still substantially wider than the limiting value determined by the YAG atomic linewidth. Active mode locking as used in this laser in general does not lead to a completely linewidth-limited pulse. A more dynamic form of mode-locking, such as is provided by a saturable absorber, is required to achieve the limiting pulsewidth. Pulsewidths as narrow as $\sim 15 \text{ psec}$ should be possible in a linewidth-limited YAG laser.

We are, therefore, now examining the possibility of adding some sort of passive pulse-shortening mechanism to our actively mode-locked laser. Analytic studies have been started, to be followed later by experiments once theoretical predictions are completed. Two approaches appear promising. One is the straightforward use of a passive saturable absorber in combination

with the active modulator. This approach will undoubtedly lead to some further pulse shortening, but it is not yet clear whether this improvement will cost more than it is worth in terms of decreased peak power output. The second approach is the use of the optical Kerr effect to produce pulse self-chirping together with an intracavity dispersive element such as a Gires-Tournois interferometer to compress the chirped pulses. This is a concept that has been considered several times for single-pass pulse compression outside of high-power lasers. It does not seem to have been explored, however, for intracavity multi-pass pulse compression. Preliminary studies show that substantial chirping should be readily obtainable, and the pulse compression stage will be evaluated next. This approach could offer very significant advantages, including very small losses and a pulse compression that increases as the pulse narrows, rather than saturating with pulse growth as does a saturable absorber.

We also intend to explore the possibilities of using the primary burst of pulses from our doubled laser to pump a synchronously mode-locked dye laser. This would give a tunable short-pulse output available in synchronism with the YAG pulses, a combination that could be ideal for practical applications including, for example, airborne optical radars for mapping algae distributions in coastal and lake waters. Substantial progress on both the above topics is intended during the next reporting period.

REFERENCES

1. D. J. Kuizenga, D. W. Phillion, Terje Lund, and A. E. Siegman, "Simultaneous Q-Switching and Mode Locking in the CW Nd:YAG Laser," *Optics Commun.* 9, 221 (November 1973).
2. A. E. Siegman and D. J. Kuizenga, "Active Mode-Coupling Phenomena in Pulsed and Continuous Lasers," *Opto-Electronics* 6, 43 (January 1974).

B. Studies Concerning the Possibility of a Li-Xe Excimer Laser

(J. H. Newton, J. F. Young, and S. E. Harris)

The goal of this project is to investigate the alkali metal excimer laser systems. In particular we have concentrated on the alkali-rare gas excimers. These excimer systems may prove to be useful as high efficiency, high power density amplifiers or lasers in the visible or near infrared portion of the spectrum.

Excimers are molecules which exist only in the excited state. The excited state exhibits an attractive potential while the ground state is repulsive. Physically, the mechanism for excimer laser action is as follows: a ground state alkali atom is excited and then combines with a ground state rare gas atom to form the molecule. When stimulated emission takes place the excimer drops to the ground state, dissociating into the free alkali and rare gas atoms. Thus the system is effectively a four-level laser, with a small energy defect.

A particularly interesting property of the alkali excimer laser systems is that a wide variety of pumping methods may be used to excite the alkali atoms. Flashlamp, electric discharge, or E-beam pumping may be used to excite the free alkali atom. For example, a typical cross section for electron excitation of alkali resonance transitions is 50 \AA^2 , which greatly exceeds other low-energy inelastic cross sections. Such pumping could offer a very efficient means of funneling energy into the upper laser level.

Initially we will use optical (laser) pumping which will allow us to excite specific levels at well known rates.

The alkali-Xe family of excimers are of most interest initially because the upper state is the most attractive relative to the other rare gases. This gives rise to greater population inversions and, hence, greater gain. Our calculations for the Na-Xe excimer indicate reasonable gain, but, unfortunately, our measurements of the Na₂ absorption indicate that the dimer absorption will dominate, preventing net gain. We have subsequently investigated the other alkali systems and have determined that, with the exception of the Li-Xe vs. Li₂, the alkali-dimer A-X band absorption extends to longer wavelengths than the alkali-rare gas excimer gain. Thus, we have concentrated our efforts on Li-Xe.

We have performed two different gain calculations which are in reasonable agreement. In the first, we calculated density distributions for the excited and ground states based on a Leonard-Jones fit to the excited state potential of Baylis¹ and a uniform potential for the ground state. Population inversions for various pump conditions, temperatures, and pressures were determined. Optical cross-sections were determined from fluorescence data. The second calculations were based on Phelps's method² using potential curves calculated by Baylis.¹ Predicted gain for Li-Xe is approximately 4% per cm for 3.90 torr Li, 2 atm Xe, and 30% excitation fraction.

Figure 1 shows a schematic of a typical laser cavity. The length l is the gain medium and d is the dead or empty space in the cavity. The net gain of the laser is $G = [c\tau_p / (l + d)] lg$, where τ_p is the pump pulse length and g is the gain per cm of the lasing medium. The gain $g = KN^*$, where K is a constant, N^* is the density of excited alkali

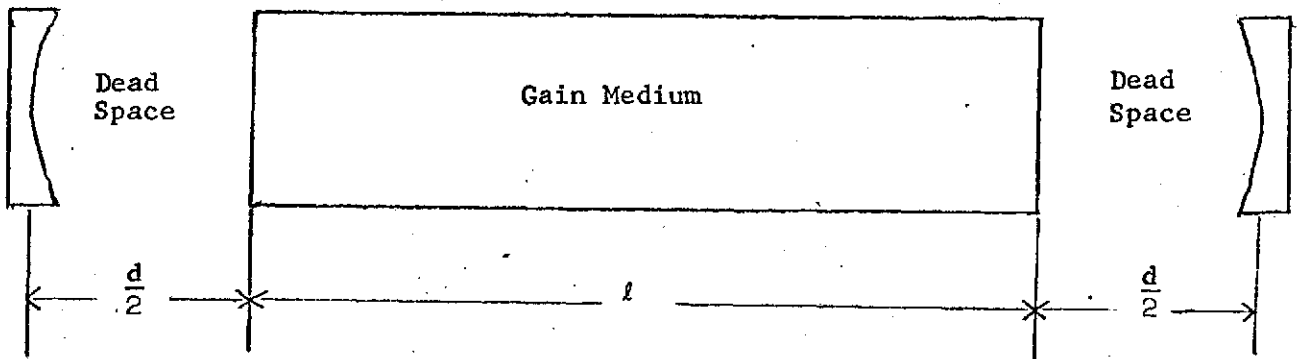


Fig. 1--Typical laser cavity.

atoms, and n_0 is the density of the rare gas. In order to achieve maximum gain, one would like the dead space d to be minimum. Thus our initial cell design had the windows of the cell in direct contact with the Li vapor, which will be at a temperature of about 1100°K . Conventional methods of sealing the windows, such as O-rings could not be used. We investigated a metalization brazing technique, but although this could probably withstand the temperature, it could not withstand the pressures. In addition, Li is extremely reactive at these high temperatures and very likely attacks both quartz and sapphire rapidly.

In view of these difficulties, we analyzed the possibilities of using a heat pipe-type design in which the windows are cold, and isolated from the vapor by a zone of pure rare gas. It is then possible to use quartz windows with O-ring seals. Such a buffer zone, however, constitutes dead space in the optical cavity which reduces net gain. The minimum buffer zone is a function of the cell temperature, pressure, and diameter. If the temperature gradient between the center of the cell and the windows is too steep, Li will condense as suspended droplets rather than on the walls which will scatter the laser beam. Emperically, the intensity of this "raining" appears to be directly proportional to the pressure, the temperature gradient in the buffer region, and inversely proportional to the cell inside diameter. From our experience with other heat pipes it seems that the temperature gradient should be limited to about $75^\circ\text{C}/(\text{diameter}) \cdot (\text{atmosphere})^{-1}$ to avoid raining. The minimum cell diameter and total length are restricted by optical diffraction considerations; the minimum temperature gradient is limited by the allowable dead space in the cavity; and the gain per pass is determined by both pressure and total cell length. A simple

mathematical model incorporating all these effects was used to design the best practical cell geometry. The cell we have constructed will have an active zone of 20 cm, with a 10 cm buffer zone on each end, and an inner diameter of 0.6 cm. It consists of a stainless steel outer tube with flanges on each end. Quartz brewster windows are sealed to the flanges with O-rings. A slotted stainless steel tube with a stainless steel wick wrapped around it is inserted in the outer tube. The cell is in the process of being loaded and tested.

To pump the Li-Xe we will use the second harmonic of the 1.338 μ line of a Nd:YAG laser. The Li resonance line is 6708 Å, but due to the Xe pressure broadening, the 6690 Å will be absorbed strongly. The calculated absorption depth is approximately 3 cm at 30% excitation of 3.90 torr Li vapor pressure and the required pump power to achieve 30% excitation for 100 ns in the above cell design is 3 kW. We will use a LiIO₃ doubling crystal and are presently assembling the pump laser.

Based on a report by York and Gallagher³ we have recently been examining the properties of a high pressure Na-Na excimer. This system is distinctly different from the low pressure Na₂ molecular laser in which ground state Na₂ molecules are directly pumped to excited states and lase to high lying ground vibrational levels. In the Na-Na excimer case ground state atoms are excited (as in alkali-rare gas excimers) and then combine with ground state Na atoms to form Na₂ (Na* + Na → Na₂*) in the presence of high pressure buffer gas. This process can be pumped much more efficiently because the ratio of Na/Na₂ is typically greater than 50. In addition, the lower melting point of Na will reduce the raining and dead space problems. We are still investigating the Na-Na excimer as well as the other alkali-

alkali excimer systems. Our present cell design should be adaptable for use with any of the alkali-alkali systems.

REFERENCES

1. W. E. Baylis, J. Chem. Phys. 51, 2665 (1969).
2. A. V. Phelps, "Tunable Gas Lasers Utilizing Ground State Dissociation," JILA Report No. 110, University of Colorado, Boulder, Colorado, 1972.
3. George York and Alan Gallagher, "High Power Gas Lasers Based on Alkali-Dimer A-X Band Radiation," JILA Report No. 114, University of Colorado, Boulder, Colorado, 1974.

C. Research Studies on Techniques for Frequency Conversion of High Power and High Energy Laser Radiation

(D. M. Bloom, J. F. Young, and S. E. Harris)

For the past period our efforts have been directed mainly at replacing the xenon formerly used as the phasematching gas with a more dispersive vapor. Experiments with a two-metal heat pipe containing sodium and mercury indicate that mercury is not a suitable metal to be used in a two-metal heat pipe with the alkali metals. The failure of the sodium-mercury heat pipe is attributed to the alloying of the metals which greatly alters their vapor pressures.

In order to understand the failure of the sodium-mercury heat pipe it is necessary to understand the general operation of a two-metal heat pipe oven. Two-metal heat pipe ovens were first proposed and demonstrated by Hessel and Jankowski¹ and later modified to allow arbitrary mixtures by Vidal and Hessel.² Detailed descriptions of the operation of this type of heat pipe oven are given in these papers. However, an important point not made in these papers and demonstrated in our experiments is that for proper operation the two fluids must be immiscible. Immiscibility is required to insure that the vapor pressures of the constituent fluids are not modified as they would be in a solution of the two.

A study of binary alloys was carried out in order to find a suitable metal which was immiscible with sodium. Magnesium was found to be immiscible with sodium, strongly positively dispersive, and has a vapor pressure similar

enough to sodium to allow operation as a two-metal heat pipe with reasonable temperature gradients. A second two-metal heat pipe oven containing sodium and magnesium was then constructed. Experimental results with this cell indicate that this heat pipe oven is operating correctly and phasematching has been obtained to as many as 50 coherence lengths. This is the first phasematched system using two metal vapors to be demonstrated and the low phasematching ratio ($N_{Mg}:N_{Na} = 1.1$) should allow operation at significantly higher sodium pressures.

Currently, experiments are underway to determine the energy conversion efficiency obtainable with the present Na:Mg heat pipe oven and a modified version is being constructed in order to obtain a more homogeneous mixture. It is hoped that these systems will allow significantly higher conversion efficiencies than previously reported.

Finally, construction of the birefringent filter is now complete and it will be installed in the laser oscillator at the conclusion of the experiments with the two-metal heat pipes. Operation of the laser at $1.074 \mu\text{m}$ should allow higher conversion efficiencies in rubidium phasematched with xenon.

REFERENCES

1. M. M. Hessel and P. Jankowski, J. Appl. Phys. 43, 209 (1972).
2. C. R. Vidal and M. M. Hessel, J. Appl. Phys. 43, 2776 (1972).

D. High Average Power Blue and UV Sources

(G. W. Bekkers, J. F. Young, and S. E. Harris)

In Appendix B of the July 1974 report it was demonstrated that in Na vapor a cw 9.26 μm CO_2 laser can be up-converted to 3321 \AA with a photon efficiency of 58%. The realization of this high conversion efficiency depends on tuning the pump frequency into exact two-photon resonance and also the incoming IR radiation has to approach resonance with the third level. This conversion efficiency is obtained in a single coherence length of metal vapor and is therefore quite broadband in both wavelength and aperture. However, the greatest advantage of this process lies in the possibility of high average power conversion. Our proposal is to use a 1.0790 μm Nd:YALO₃ laser which is exactly resonant with the 6s-7s transition in Cs and up-convert a 3 μm chemical laser line to 4556 \AA .

The maximum power density which can be used in two-photon resonantly pumped processes is limited by two-photon absorption under the condition that $W^{(2)}\tau = 1/2$, where τ is either the incident laser pulse length Δt or the decay time T_1 of the second level, whichever is shorter. In Appendix A of the January 1974 report the last coherence length power conversion efficiency ϵ was calculated for the case that the coherence length is set by the upper level and the power density is limited by two-photon absorption:

$$\epsilon = \frac{2}{\tau \omega_2} \frac{\mu_{23}^2}{\mu_{03}^2},$$

where the μ 's are the dipole moments between levels indicated by the subscripts and $\delta\omega_2$ is the half-power linewidth of the two-photon transition. \mathcal{E} is the power conversion efficiency of the incoming IR radiation into the generated UV or blue radiation. It is generally assumed that forbidden transitions like s-s or s-d are only lifetime broadened but dephasing collisions might cause pressure broadening. We were not able to find any literature on the broadening mechanism of these unallowed transitions. Therefore in our calculations we have to introduce an uncertainty range of $\delta\omega_2 = 5.3 \times 10^{-4} \text{ cm}^{-1}$ in case of lifetime broadening to a maximum of $\delta\omega_2 = 0.1 \text{ cm}^{-1}$ in case of pressure broadening. Even in the latter case a power up-conversion efficiency $\mathcal{E} = 200\%$ can be achieved. In case of third harmonic generation we can use the expression for \mathcal{E} given in the July 1974 report together with the condition $W^{(2)}\tau = 1/2$. This leads to an expected power conversion efficiency of 0.4% in one coherence length in case of lifetime broadening. In case of maximum pressure broadening this number is reduced by the square root of the ratios of $\delta\omega_2$. The result is a conversion efficiency of 0.029%.

A heat pipe is a device in which a chemical substance is evaporated in the center of a pipe and then condenses at the ends giving off its latent heat. The liquid substance is returned to the center by means of a wick. By filling the ends of the pipe with an inert gas the vapor pressure of the substance can be controlled. The great advantages of this device are the constant temperature along the pipe and the fact that the substance does not touch the windows. A stainless steel heat pipe using Cs vapor with argon as an inert gas is presently in operation at pressures from 1-60 mm Hg. The wick is made from fine stainless steel mesh.

When crystals are inserted in a laser cavity the maximum average power of the doubled frequency can reach 2W. An example is a LiIO_3 crystal inserted into a Nd:YAG laser cavity running on the 0.946 line which delivers 0.3 W average power (Chromatix). These systems can achieve a 40-50% doubling efficiency. Up-conversion in heat pipes can also achieve this conversion efficiency and at the same time much higher average powers can be obtained. This is due to the high speed with which the alkaline atoms travel through the heat pipe. When atoms leave the evaporation zone, which is centered under the heating element, they enter the condensation zone. The nonlinear process only takes place in the evaporation zone where the density of atoms is constant. It has been determined that at the interface between evaporation zone and condensation zone the velocity of the atoms can be subsonic. For 10 torr of Cs vapor the sonic speed is around 250 m/sec. This means that for a 1.5 cm long zone all atoms are replenished inbetween laser pulses up to high pulse repetition rates. Therefore if a high conversion efficiency can be achieved in one pulse, then high average power conversion is also possible, e.g., a 1.5 cm long zone, a 0.5 cm laser beam diameter, a typical power density of $5 \times 10^6 \text{ W/cm}^2$ and a 50 nsec pulse leads to a 17 W average power 4556 \AA radiation in Cs vapor at 1000 pps. The pulse length can even be much longer.

At the moment the biggest unknown is the linewidth $\delta\omega_2$ of the two-photon transition. This linewidth can be calculated by measuring two-photon absorption at several operating points, since all other quantities are accurately known. Once $\delta\omega_2$ is known we can verify its value by measuring third harmonic generation. The next step is to up-convert a tunable $3 \mu\text{m}$

source and verify the results with theory. When the outcome of this experiment is successful then high average power conversion using a 3 μm chemical laser should be attempted.

We started out, not with a heat pipe, but with a 0.5 cm long stainless steel cell with sapphire windows at the ends and loaded with Cs. The cell was heated several times to 450°C without any side effects. However, when the Nd:YALO₃ laser was propagated through the cell, the sapphire windows showed a black deposition around the location where the laser beam passed. The area of this deposition was 10-100 times larger than the beam area at that location. A telephone conversation with J. Reintjes at the Naval Research Laboratory in Washington, who is measuring self-defocusing in Cs vapor at 1.06 μm , revealed that he also observed this deposition. These two independent observations make it unlikely that any contamination is involved. The physical origin of this deposition has not yet been pinpointed.

The discovery of the near coincidence of two Nd:YALO₃ photons at 1.0795 μm and the 6s-7s transition in Cs led to a search for exact resonance. A smaller detuning from the second level means that a certain conversion efficiency can be achieved at a lower power density. Measuring the Nd:YALO₃ fluorescence spectrum showed that the desired 1.0790 μm wavelength was at the 40% level. By inserting an etalon into the laser cavity the Nd:YALO₃ laser now can be tuned over the range 1.0799 \rightarrow 1.0789 μm , delivering up to 3 mJ per 50 nsec pulse.

The first experiment was aimed at carefully measuring two-photon absorption and calculating $\delta\omega_2$ from these data. Two-photon absorption can be

distinguished from linear atomic absorption by its power dependence and from linear molecular absorption by its temperature dependence. At an atomic density of 2×10^{17} atoms per cc we measured a molecular Cs_2 absorption of 50% in a 1.5 cm long zone. When the power density was increased a new phenomenon occurred. The number of atoms in the volume of the laser beam is known and since only one-half of these atoms can be excited to the 7s level the maximum two-photon absorption is determined. However, the total absorbed energy was about 50 times higher than this maximum amount and showed two peaks about 1.7 cm^{-1} wide and separated by 3.5 cm^{-1} . From the observation of a threshold and the amount of loss we concluded this to be the result of a four-wave parametric oscillation; but a careful scan of the output spectrum did not reveal any of the two additional wavelengths. These two losses overshadowed the two-photon absorption, so that this experiment was inconclusive for $\delta\omega_2$. As a consequence we have to operate the Cs heat pipe at a few torr where the ratio of molecules to atoms is small and at power densities below the threshold of above described effect.

While the Nd:YAlO_3 laser was tuned over its $1.0799 \rightarrow 1.0789 \text{ }\mu\text{m}$ range the third harmonic generation peaked at the expected $1.0790 \text{ }\mu\text{m}$ wavelength. The measured value was $10^{-4} - 10^{-3}$ percent at the peak and the full width at half power was 1 cm^{-1} . This is wider than one would expect from a 0.3 cm^{-1} wide laser line.

The experiment which is set up at the moment is to add the tunable output around $3 \text{ }\mu\text{m}$ of an optical parametric oscillator to the Nd:YAlO_3 input. The oscillator contains a 4 cm LiNbO_3 crystal which is pumped by a doubled $1.0790 \text{ }\mu\text{m}$. This doubling is done in a CDA crystal. Tuning of the

oscillator is performed by changing the crystal temperature. The two beams are fed collinearly into the Cs heat pipe. Measurements of the up-conversion efficiency vs. wavelength are currently underway.

APPENDIX A

EFFECTS OF FOCUSING ON THIRD-ORDER NONLINEAR
PROCESSES IN ISOTROPIC MEDIA*

by

Gary C. Bjorklund[†]

Microwave Laboratory
Stanford University
Stanford, California 94305

ABSTRACT

A theoretical analysis of third-order nonlinear interactions of focused laser beams is performed for the processes $\omega_1 + \omega_2 + \omega_3 \rightarrow \omega_4$, $\omega_1 + \omega_2 - \omega_3 \rightarrow \omega_4$, and $\omega_1 - \omega_2 - \omega_3 \rightarrow \omega_4$. The total power and far-field beam profile of the generated radiation is related to the total powers of the fundamental beams, to the tightness and location of the focus, and to the value of the difference between the wave vectors of the generated radiation and driving polarization. The optimum degree of wave vector mismatch as a function of tightness and location of focus is determined for each of the three processes. The process $\omega_1 + \omega_2 - \omega_3 \rightarrow \omega_4$ is found to be unique in that it is always optimized by focusing as tightly as possible. Experimental results, which verify the theory for the processes $\omega_1 + \omega_2 + \omega_3 \rightarrow \omega_4$ and $\omega_1 + \omega_2 - \omega_3 \rightarrow \omega_4$, are presented.

*Work supported by the National Aeronautics and Space Administration.

[†]Present address: Bell Telephone Laboratories, Holmdel, New Jersey 07733, (201) 949-4917.

EFFECTS OF FOCUSING ON THIRD-ORDER NONLINEAR
PROCESSES IN ISOTROPIC MEDIA

by

Gary C. Bjorklund
Microwave Laboratory
Stanford University
Stanford, California 94305

I. INTRODUCTION

Third-order nonlinear processes in isotropic media have recently been utilized for efficient frequency tripling of high power laser radiation,^{1,2} for the production of tunable^{3,4} and fixed frequency^{5,6} coherent vacuum ultraviolet radiation, for up-conversion of infrared radiation,^{7,8} for the production of tunable infrared radiation,⁹ and for coherent anti-Stokes Raman spectroscopy.¹⁰⁻¹³ These processes involve frequency sum and/or difference mixing between as many as three different fundamental frequencies. In order to achieve the high power densities required by these processes without damaging the windows of the cell containing the nonlinear medium, it is often necessary to focus the fundamental beams tightly enough to produce a depth of focus small in comparison to the cell length. Focusing in this manner dramatically alters the form of the functional dependence of the efficiencies on the mismatch between the wave vectors of the generated radiation and driving polarization.

This paper presents a theoretical and experimental investigation of the effects of focusing on the processes $\omega_1 + \omega_2 + \omega_3 \rightarrow \omega_4$, $\omega_1 + \omega_2 - \omega_3 \rightarrow \omega_4$, and $\omega_1 - \omega_2 - \omega_3 \rightarrow \omega_4$. The optimum values of the wave vector mismatch, Δk (defined as the wave vector of the generated radiation minus the wave vector of the driving polarization), are found to depend on the tightness and location of the focus. In the case of very tight focusing with the fundamental beam waist region entirely contained within the cell, efficient generation can be achieved only for restricted values of Δk . It is shown that Δk must be non-zero and negative for the process $\omega_1 + \omega_2 + \omega_3 \rightarrow \omega_4$ and that Δk must be non-zero and positive for the process $\omega_1 - \omega_2 - \omega_3 \rightarrow \omega_4$. Given a nonlinear medium with dispersion characteristics proper to produce the correct sign for Δk , each of these processes can be optimized by varying the tightness of focus. The process $\omega_1 + \omega_2 - \omega_3 \rightarrow \omega_4$ is found to be unique in that it can always be optimized by varying the tightness of focus, regardless of the dispersion characteristics of the nonlinear medium.

These focusing effects arise from the well known phase shift of π radians which occurs as a beam traverses the region of the focus. This phase shift also affects the driving polarization and, except for the process $\omega_1 + \omega_2 - \omega_3 \rightarrow \omega_4$, introduces a slip in phase between the driving polarization and the generated radiation. Destructive interference between portions of the generated radiation arising from different locations in the cell will result unless this slip in phase is compensated by a wave vector mismatch of the proper sign.

In the following sections, a rigorous theoretical analysis is used to derive expressions which relate the total power and far-field beam profile of the generated radiation to the total powers of the fundamental beams, to

the tightness and location of focus of these beams relative to the dimensions of the cell, and to the value of the wave vector mismatch. Numerical evaluations of these expressions are presented for a wide variety of cases. Procedures for the optimization of the total generated power are discussed. Experimental results, which verify some aspects of the theory, are presented.

It should be noted that the effects of focusing in the case of third harmonic generation in isotropic media have been previously considered by Miles and Harris¹ and by Ward and New.¹⁴ The rigorous theoretical analysis of this paper is an extension of the work of Ward and New and of Kleinman, et al.¹⁵

II. THEORY

In this section, expressions are developed for the total output power and beam shape of the generated radiation produced by the four-wave mixing processes $\omega_1 + \omega_2 + \omega_3 \rightarrow \omega_4$, $\omega_1 + \omega_2 - \omega_3 \rightarrow \omega_4$, and $\omega_1 - \omega_2 - \omega_3 \rightarrow \omega_4$. The basic approach is to specify the spatial variation of the driving polarization, perform a Fourier decomposition of the driving polarization into plane wave components, calculate the generated radiation field arising from each such component, and then to determine the total generated field by summing the contributions of all of these components.

The fundamental beams at ω_1 , ω_2 , and ω_3 are assumed to be lowest order Gaussian modes which propagate concentrically along the z axis with identical waist locations and identical confocal beam parameters. If the wave vectors of these beams in the nonlinear medium are taken as k_1 , k_2 , and k_3 respectively, and if the electric field amplitudes are taken as \vec{E}_{10} , \vec{E}_{20} , and \vec{E}_{30} respectively, then the fundamental electric field is given by

$$\vec{E}(\vec{r}, t) = \text{Re} \left[\vec{E}_1(\vec{r}) e^{-i\omega_1 t} + \vec{E}_2(\vec{r}) e^{-i\omega_2 t} + \vec{E}_3(\vec{r}) e^{-i\omega_3 t} \right] \quad (1)$$

with \vec{E}_n , where $n = 1, 2, \text{ or } 3$, given by the theory of Boyd and

Gordon¹⁶ as

$$\vec{E}_n(\vec{r}) = \vec{E}_{n0} \exp(ik_n z) (1 + i\mathcal{E})^{-1} \exp \left[-k_n (x^2 + y^2) / b(1 + i\mathcal{E}) \right] \quad (2)$$

In Eq. (2), b is the confocal parameter, defined by

$$b = \frac{2\pi\omega_0^2}{\lambda} = \frac{2\pi\omega_0^2 n}{\lambda_0} = \frac{2\lambda_0}{n\theta^2} = k\omega_0^2, \quad (3)$$

where ω_0 is the beam waist radius, n is the index of refraction, λ_0 is the vacuum wavelength, and θ is the far-field diffraction half angle. \mathcal{E} is a normalized coordinate along the z axis, defined as

$$\mathcal{E} = \frac{2(z - f)}{b}, \quad (4)$$

where f is the position of the focus (beam waist) along the z axis.

If the fundamental and generated beams are all assumed to be linearly polarized in the same direction, the vector nature of the electric fields as well as the tensor nature of the nonlinear susceptibility may be neglected, and the driving polarization of ω_4 is given by

$$P_4(\vec{r}, t) = \text{Re} \left[P_4(\vec{r}) e^{-i\omega_4 t} \right], \quad (5)$$

where

$$P_4(\vec{r}) = \left\{ \begin{array}{l} \frac{3}{2} NX (-\omega_4; \omega_1, \omega_2, \omega_3) E_1(\vec{r}) E_2(\vec{r}) E_3(\vec{r}) \\ \quad (\text{for } \omega_1 + \omega_2 + \omega_3 \rightarrow \omega_4) \\ \frac{3}{2} NX (-\omega_4; \omega_1, \omega_2, -\omega_3) E_1(\vec{r}) E_2(\vec{r}) E_3^*(\vec{r}) \\ \quad (\text{for } \omega_1 + \omega_2 - \omega_3 \rightarrow \omega_4) \\ \frac{3}{2} NX (-\omega_4; \omega_1, -\omega_2, -\omega_3) E_1(\vec{r}) E_2^*(\vec{r}) E_3^*(\vec{r}) \\ \quad (\text{for } \omega_1 - \omega_2 - \omega_3 \rightarrow \omega_4) \end{array} \right. , \quad (6)$$

with χ the nonlinear susceptibility per atom and N the number density of atoms of the nonlinear medium. [When two or three of the input frequencies are degenerate, the factor of $\frac{3}{2}$ in Eq. (6) must be changed to $\frac{3}{4}$ or $\frac{1}{4}$ respectively.]

The nonlinear medium is considered to occupy the semi-infinite space $z > 0$, with the space $z < 0$ considered to be a vacuum. Then from Eqs. (2) and (6), for the process $\omega_1 + \omega_2 + \omega_3 \rightarrow \omega_4$, the driving polarization at ω_4 is given by

$$P_4(\vec{r}) = \frac{3}{2} NX (-\omega_4; \omega_1, \omega_2, \omega_3) E_{10} E_{20} E_{30} \times \exp(ik'z)(1+i\mathcal{E})^{-3} \exp\left[\frac{-k'(x^2+y^2)}{b(1+i\mathcal{E})}\right] B(z) , \quad (7)$$

where k' , the wave vector of the driving polarization, is given by

$$k' = k_1 + k_2 + k_3 = k'' \quad , \quad (8)$$

and where

$$B(z) = \begin{cases} 1 & z > 0 \\ 0 & z < 0 \end{cases} \quad . \quad (9)$$

Similarly, for the process $\omega_1 + \omega_2 - \omega_3 \rightarrow \omega_4$,

$$P_4(\vec{r}) = \frac{3}{2} N \chi(-\omega_4; \omega_1, \omega_2, -\omega_3) E_{10} E_{20} E_{30} B(z) \\ \times \exp(ik'z)(1+i\epsilon)^{-2}(1-i\epsilon)^{-1} \exp\left[\frac{(-k'' + i\epsilon k')(x^2 + y^2)}{b(1 + \epsilon^2)}\right] \quad , \quad (10)$$

where k' is now defined as

$$k' = k_1 + k_2 - k_3 \quad , \quad (11)$$

and k'' is defined as before.

Finally, for the process $\omega_1 - \omega_2 - \omega_3 \rightarrow \omega_4$,

$$P_4(\vec{r}) = \frac{3}{2} N \chi(-\omega_4; \omega_1, -\omega_2, -\omega_3) E_{10} E_{20} E_{30} B(z) \\ \times \exp(ik'z)(1+i\epsilon)^{-1}(1-i\epsilon)^{-2} \exp\left[\frac{(-k'' + i\epsilon k')(x^2 + y^2)}{b(1 + \epsilon^2)}\right] \quad , \quad (12)$$

where k' is now defined as

$$k' = k_1 - k_2 - k_3, \quad (13)$$

and k'' is defined as before.

The next step is to perform a Fourier decomposition of $P_4(\vec{r})$ to determine the amplitudes of the plane wave components of the driving polarization. $P_4(\vec{K})$, the amplitude of the plane wave component with wave vector \vec{K} , is defined by

$$P_4(\vec{K}) = (2\pi)^{-3} \int_{-\infty}^{\infty} dx'' \int_{-\infty}^{\infty} dy'' \int_{-\infty}^{\infty} dz'' P_4(\vec{r}'') \exp(-i\vec{K} \cdot \vec{r}'') \quad (14)$$

$\vec{E}_4(\vec{K})(\vec{r})$, the generated radiation field arising from the plane wave component of the driving polarization with wave vector \vec{K} , and $\vec{P}_4(\vec{K})$ can be shown by Maxwell's Equations to be related by

$$\vec{\nabla} \times \vec{\nabla} \times \vec{E}_4(\vec{K})(\vec{r}) - k_4^2 \vec{E}_4(\vec{K})(\vec{r}) = 4\pi k_0^2 \vec{P}_4(\vec{K}) \exp(i\vec{K} \cdot \vec{r}) \quad (15)$$

where k_4 and k_0 are the wave vectors of the generated radiation in the nonlinear medium and in vacuum respectively. Equation (15) may be solved subject to the boundary condition that the tangential component of $\vec{E}_4(\vec{K})$ vanish at the vacuum-medium interface. For $K_x, K_y \ll K_z$ and $|\vec{K}| - k_4 \ll |\vec{K}|$, k_4 , Kleinman¹⁷ has shown that

$$E_4(\vec{K})(\vec{r}) = i[2\pi k_0^2 z / k_4] g(U_{\vec{K}}) \exp(i\vec{K} \cdot \vec{r}) P_4(\vec{K}) \quad (16)$$

with

$$U_{\vec{K}} = iz [K_z - k_4 + (K_x^2 + K_y^2)/2k_4] \quad , \quad (17)$$

and

$$g(x) = [1 - \exp(-x)]/x = \int_0^1 e^{-xp} dp \quad . \quad (18)$$

The wave vector mismatch, Δk , is defined by the relation

$$\Delta k = k_4 - k' \quad . \quad (19)$$

This choice of sign for Δk is opposite from that of Ward and New¹⁴ but consistent with Miles and Harris.¹

The substitutions $k_4 = k' + \Delta k$ and $p = -\frac{1}{2} b(\mathcal{E}' - \mathcal{E})/z$ may be performed in Eqs. (17) and (18) to yield (assuming $\Delta k \ll k_4, k'$)

$$g(U_{\vec{K}}) = \left(\frac{b}{2z}\right) \int_{-\zeta}^{\mathcal{E}} d\mathcal{E}' \exp \left\{ ib [K_z - k' + (K_x^2 + K_y^2)/2k' - \Delta k] (\mathcal{E}' - \mathcal{E})/2 \right\} \quad , \quad (20)$$

where $\mathcal{E} = 2(z - f)/b$ and $\zeta = 2f/b$.

The total generated electric field, $E_4(\vec{r})$, is derived by combining the $E_4(\vec{K})(\vec{r})$,

$$E_4(\vec{r}) = \int_{-\infty}^{\infty} dK_x \int_{-\infty}^{\infty} dK_y \int_{-\infty}^{\infty} dK_z E_4(\vec{K})(\vec{r}) \quad , \quad (21)$$

where $E_4(\vec{K})(\vec{r})$ is defined by Eqs. (16), (20), and (14).

These integrals may be evaluated by first integrating over K_z to yield the factor $\delta(z'' - z)$, then integrating over z'' , and finally integrating over x'' , y'' , K_x , and K_y by means of the formula¹⁵

$$\int_{-\infty}^{\infty} \exp[-iqx - isx^2] dx = (\pi/is)^{\frac{1}{2}} \exp(iq^2/4s) \quad \text{Im}(s) < 0 \quad (22)$$

For $\omega_1 + \omega_2 + \omega_3 \rightarrow \omega_4$, the result is

$$E_4(\vec{r}) = i \frac{3N}{2k_4} \pi k_0^2 b \chi(-\omega_4; \omega_1, \omega_2, \omega_3) E_{10} E_{20} E_{30} \exp(ik'z)(1+i\epsilon)^{-1} \\ \times \exp\left[\frac{-k'(x^2+y^2)}{b(1+i\epsilon)}\right] \cdot \int_{-\xi}^{\epsilon} \frac{\exp[-(ib/2) \Delta k (\epsilon' - \epsilon)]}{(1+i\epsilon')^2} d\epsilon' \quad (23)$$

while for $\omega_1 + \omega_2 - \omega_3 \rightarrow \omega_4$,

$$E_4(\vec{r}) = i \frac{3N}{2k_4} \pi k_0^2 b \chi(-\omega_4; \omega_1, \omega_2, -\omega_3) E_{10} E_{20} E_{30} \exp(ik'z) \\ \times \int_{-\xi}^{\epsilon} d\epsilon' \frac{\exp[-(ib/2) \Delta k (\epsilon' - \epsilon)]}{(1+i\epsilon')(k'' - ik'\epsilon')H} \exp\left[\frac{-(x^2+y^2)}{bH}\right] \quad (24)$$

and for $\omega_1 - \omega_2 - \omega_3 \rightarrow \omega_4$,

$$E_4(\vec{r}) = i \frac{3N}{2k_4} \pi k_0^2 b \chi(-\omega_4; \omega_1, -\omega_2, -\omega_3) E_{10} E_{20} E_{30} \exp(ik'z) \\ \times \int_{-\xi}^{\xi} d\varepsilon' \frac{\exp[-(ib/2)\Delta k(\varepsilon' - \varepsilon)]}{(1 - i\varepsilon')(k'' - ik'\varepsilon')H} \exp\left[\frac{-(x^2 + y^2)}{bH}\right] \quad (25)$$

k' is defined by Eqs. (8), (11), and (13) in Eqs. (23), (24), and (25) respectively. k'' is always given by Eq. (8) and the function H is defined by

$$H = H(\varepsilon, \varepsilon') = \frac{(1 + \varepsilon'^2)}{(k'' - ik'\varepsilon')} - i \frac{(\varepsilon' - \varepsilon)}{k'} \quad (26)$$

If the nonlinear medium is contained in a cell of length L with input window located at $z = 0$ and with the location of the focus at $z = f$, then Eqs. (23), (24), and (25), with $\varepsilon = 2(L-f)/b$, $z = L$, and $\xi = 2f/b$, completely describe the amplitude of the generated field at the plane of the output window. The functional dependence of the field distribution upon the transverse coordinates x and y scales with the value of k' , b , and ε .

It can be seen from Eq. (23) that for the process $\omega_1 + \omega_2 + \omega_3 \rightarrow \omega_4$, $E_4(\vec{r})$ is always a lowest order Gaussian mode with the same confocal parameter and waist location as the input beams. However, Eqs. (24) and (25) show that for the processes $\omega_1 + \omega_2 - \omega_3 \rightarrow \omega_4$ and $\omega_1 - \omega_2 - \omega_3 \rightarrow \omega_4$, $E_4(\vec{r})$ is not in general a single Gaussian mode except when $k'' = k'$. The multimode output of the difference

mixing processes may be explained as resulting from a mismatch between the size of the driving polarization beam waist and the size of the generated radiation beam waist which would correspond to the confocal parameter of the input beams. This mismatch may be represented by the ratio k''/k' . When $k''/k' = 1$, these beam waists are of the same size, and a lowest order Gaussian beam with the same confocal parameter and waist location as the input beams can be produced. The sum mixing process $\omega_1 + \omega_2 + \omega_3 \rightarrow \omega_4$ always has $k''/k' = 1$ and thus always produces a lowest order Gaussian beam output.

For all three mixing processes it may be seen that $E_4(\vec{r})$ is circularly symmetrical about the z axis and that the total generated power at ω_4 is thus obtained by performing integrals of the form

$$\int_0^{\infty} 2\pi R |E(\vec{R})|^2 dR, \quad (27)$$

where $R = (x^2 + y^2)^{\frac{1}{2}}$. It is convenient to define the dimensionless functions $F_j(b\Delta k, \frac{b}{L}, \frac{f}{L}, \frac{k''}{k'})$ by the relations

$$F_j \left(b\Delta k, \frac{b}{L}, \frac{f}{L}, \frac{k''}{k'} \right) = \frac{8}{9} \frac{k_4^2 k'}{\pi^3 k_0^4} \frac{1}{b^3 X^2 |E_{10} E_{20} E_{30}|^2} \times \int 2\pi R |E(R)|^2 dR, \quad (28)$$

where $j = 1, 2, \text{ or } 3$ implies $\omega_1 + \omega_2 + \omega_3 \rightarrow \omega_4$, $\omega_1 + \omega_2 - \omega_3 \rightarrow \omega_4$, or $\omega_1 - \omega_2 - \omega_3 \rightarrow \omega_4$. Although the spatial distribution of $E_4(\vec{r})$ depends upon the value and units of k' and b' , the integrated intensity represented by the F_j depends only on the dimensionless parameters $b\Delta k$, b/L , f/L , and k''/k' .

With all wave vectors expressed in units of cm^{-1} , b in cm , N in atoms/cm^3 , χ in e.s.u. per atom, and with total power in watts, the total generated power, P_4 , is given by

$$P_4 = (6.318 \times 10^{-4}) \frac{k_0^4 k_1^2 k_2^2 k_3^2}{k_4^2 k'} N^2 \chi^2 P_1 P_2 P_3 \cdot F_j \left(b\Delta k, \frac{b}{L}, \frac{f}{L}, \frac{k''}{k'} \right), \quad (29)$$

where P_1 , P_2 , and P_3 are the total powers of each of the fundamental beams.

For the process $\omega_1 + \omega_2 + \omega_3 \rightarrow \omega_4$,

$$F_1 \left(b\Delta k, \frac{b}{L}, \frac{f}{L}, \frac{k''}{k'} \right) = \left| \int_{-\xi}^{\xi} d\mathcal{E} \frac{\exp[-(ib/2)\Delta k \mathcal{E}']}{(1+i\mathcal{E}')^2} \right|^2. \quad (30)$$

Thus $F_1(b\Delta k, b/L, f/L, 1)$ is equivalent to the quantity $|I(\beta, \Delta k, \mathcal{E}, \xi)|^2$ as defined by Ward and New¹⁴ (who define Δk with the opposite sign). In the tight focusing limit where b is short compared to the cell, and the entire focal region is contained within the cell ($\mathcal{E}, \xi \rightarrow \infty$), the integral may be solved in closed form to yield

$$F_1(b\Delta k, 0, 0.5, 1) = \begin{cases} \pi^2 (b\Delta k)^2 \exp[b\Delta k/2] & \text{for } \Delta k < 0 \\ 0 & \text{for } \Delta k \geq 0 \end{cases}. \quad (31)$$

For the process $\omega_1 + \omega_2 - \omega_3 \rightarrow \omega_4$,

$$\begin{aligned}
 F_2 \left(b\Delta k, \frac{b}{L}, \frac{f}{L}, \frac{k''}{k'} \right) &= \frac{2k'}{\pi b} \int_0^\infty 2\pi R dR \\
 &\times \left| \int_{-\xi}^{\xi} d\mathcal{E}' \frac{\exp[-(ib/2)\Delta k \mathcal{E}']}{(1+i\mathcal{E}')(k''-ik'\mathcal{E}')H} \right. \\
 &\times \left. \exp \left[\frac{-R^2}{bH} \right] \right|^2, \quad (32)
 \end{aligned}$$

with H defined by Eq. (26) and k' and k'' defined by Eqs. (8) and (11). In the tight focusing limit and in the case $k'' = k'$,

$$F_2(b\Delta k, 0, 0.5, 1) = \pi^2 \exp[-b|\Delta k|] \quad (33)$$

For the process $\omega_1 - \omega_2 - \omega_3 \rightarrow \omega_4$,

$$\begin{aligned}
 F_3 \left(b\Delta k, \frac{b}{L}, \frac{f}{L}, \frac{k''}{k'} \right) &= \frac{2k'}{\pi b} \int_0^\infty 2\pi R dR \\
 &\times \left| \int_{-\xi}^{\xi} d\mathcal{E}' \frac{\exp[-(ib/2)\Delta k \mathcal{E}']}{(1-i\mathcal{E}')(k''-ik'\mathcal{E}')H} \right. \\
 &\times \left. \exp \left[\frac{-R^2}{bH} \right] \right|^2, \quad (34)
 \end{aligned}$$

with H defined by Eq. (26) and k' and k'' defined by Eqs. (8) and (13). In the tight focusing limit and in the case $k'' = k'$,

$$F_3(b\Delta k, 0, 0.5, 1) = \begin{cases} 0 & \text{for } \Delta k \leq 0 \\ \pi^2 (b\Delta k)^2 \exp [b\Delta k/2] & \text{for } \Delta k > 0 \end{cases} \quad (35)$$

III. EVALUATION OF THE F_j

The functions F_j were numerically evaluated as continuous functions of $b\Delta k$ for various sets of discrete values of b/L , f/L , and k''/k' . From Eqs. (30), (32), and (34) it is evident that the evaluation of each F_j involves an integration over \mathcal{E}' which may be put in the form of a Fourier transformation. An efficient discrete Fast Fourier Transform routine¹⁹ was employed to numerically evaluate the F_j on an IBM computer. This routine is capable of performing a 4096 element complex discrete Fourier Transform in less than 4 seconds of computer time. One such transformation is sufficient to completely specify F_1 as a function of $b\Delta k$ for one set of values of b/L and f/L , or to evaluate $|E_h(\vec{R})|^2$ as a function of $b\Delta k$ for one set of values of b/L , f/L , k''/k' , and R . F_2 and F_3 were calculated as functions of $b\Delta k$ for one set of values of b/L , f/L , and k''/k' by evaluating $|E_h(\vec{R})|^2$ for 40 discrete values of R and then integrating over R by means of the trapezoidal rule. Thus the determination of F_2 or F_3 as a function of $b\Delta k$ for a single set of values of b/L , f/L , and k''/k' required the Fast Fourier Transform routine to be run 40 times and required approximately 3 minutes of computer time.

The behavior of the F_j near the tight focusing limit was studied in detail. It was determined that, when $b/L \leq 0.1$ and when $b \leq f \leq L - b$,

the F_j as functions of $b\Delta k$ may, to a good approximation, be represented by the curve for F_j vs. $b\Delta k$ corresponding to the infinitely tight focusing limit where $b/L = 0.0$ and $f/L = 0.5$. For instance, the maximum deviation of the numerically computed $F_1(b\Delta k, 0.1, 0.5, 1)$ from the analytically derived $F_1(b\Delta k, 0, 0.5, 1)$ of Eq. (31) is less than 0.1 for all values of $b\Delta k$.

F_1 for $b/L \leq 0.1$ and $f/L = 0.5$ is plotted in Fig. 1; F_2 for $b/L \leq 0.1$, $f/L = 0.5$, and $k''/k' = 1, 1.1, 1.5, 2.0$, and 3.0 are plotted in Fig. 2; and F_3 for $b/L \leq 0.1$, $f/L = 0.5$, and $k''/k' = 1, 1.1, 1.5, 2.0$ and 3.0 are plotted in Fig. 3. The analytical results of Eqs. (31), (33), and (35) were used to supply the curves for $b/L = 0$, while the numerical results were used for $b/L \neq 0$.

In the case of tight focusing, the F_j , when viewed as functions of $b\Delta k$, have the mutual characteristic of possessing a single large peak. As the value of $b\Delta k$ departs from the optimum value, the F_j approach zero in a nearly asymptotic manner. In the case of b/L slightly more than zero, some sidelobe structure appears far in the wings. However, as long as the fundamental beam waist region is contained entirely in the cell, these sidelobes are always less than 0.1% of the magnitude of the peak value of F_j . (This is in distinct contrast to the plane wave case, where sidelobes to the main peak occur with magnitudes as high as 4% of the maximum value.) The magnitudes and locations of the peaks of the F_j are given in Table I.

In the case of very loose focusing, the F_j approach the plane wave limit, as given by Miles and Harris,¹ of

$$\lim_{b/L \rightarrow \infty} F_j \left(b\Delta k, \frac{b}{L}, 0.5, \frac{k''}{k'} \right) = \frac{4L^2}{b^2} \text{sinc}^2 \left(\frac{\Delta k L}{2} \right) \quad (36)$$

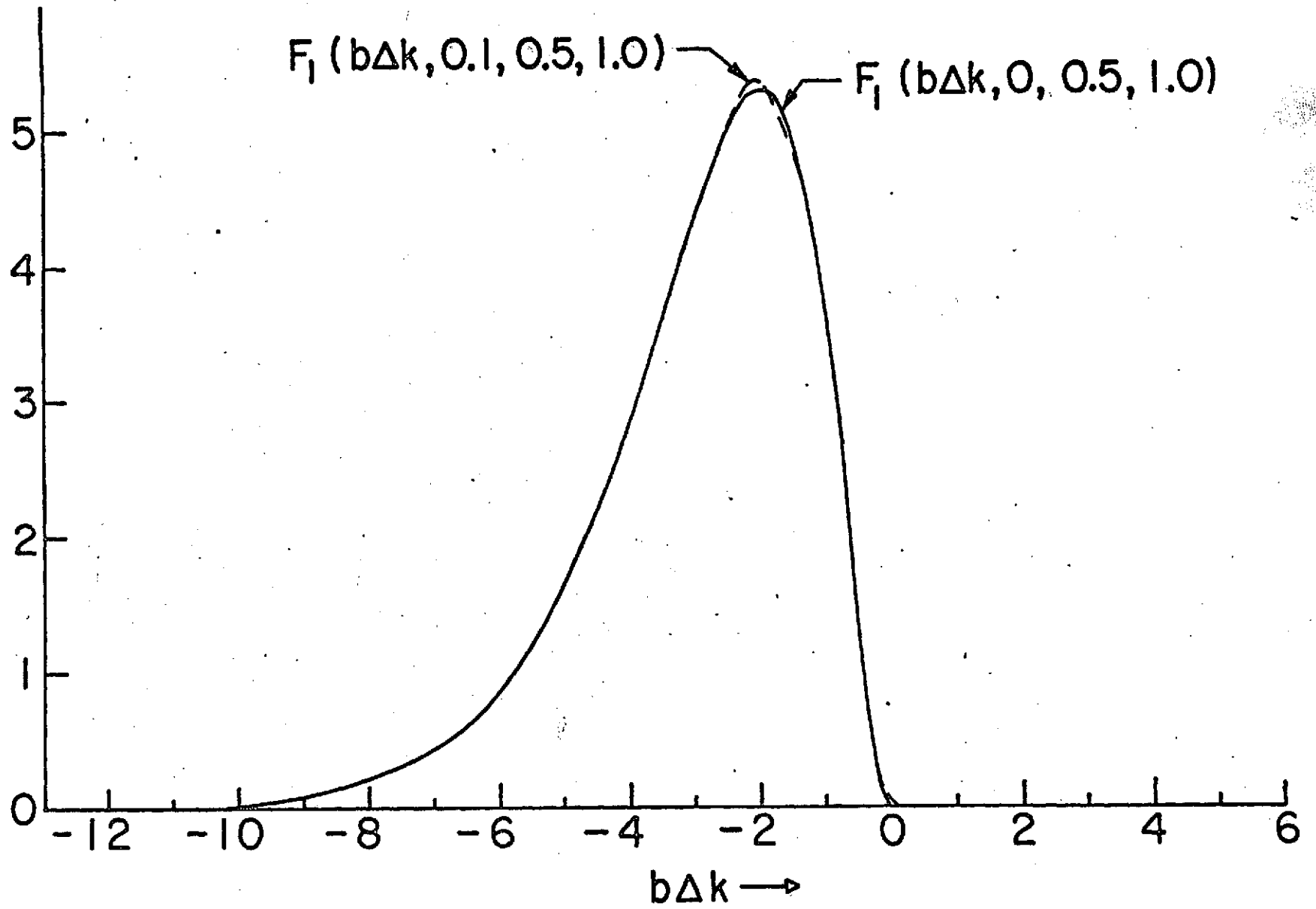


Fig. 1-- F_1 vs. $b\Delta k$ for $b/L \leq 0.1$ and $f/L = 0.5$.

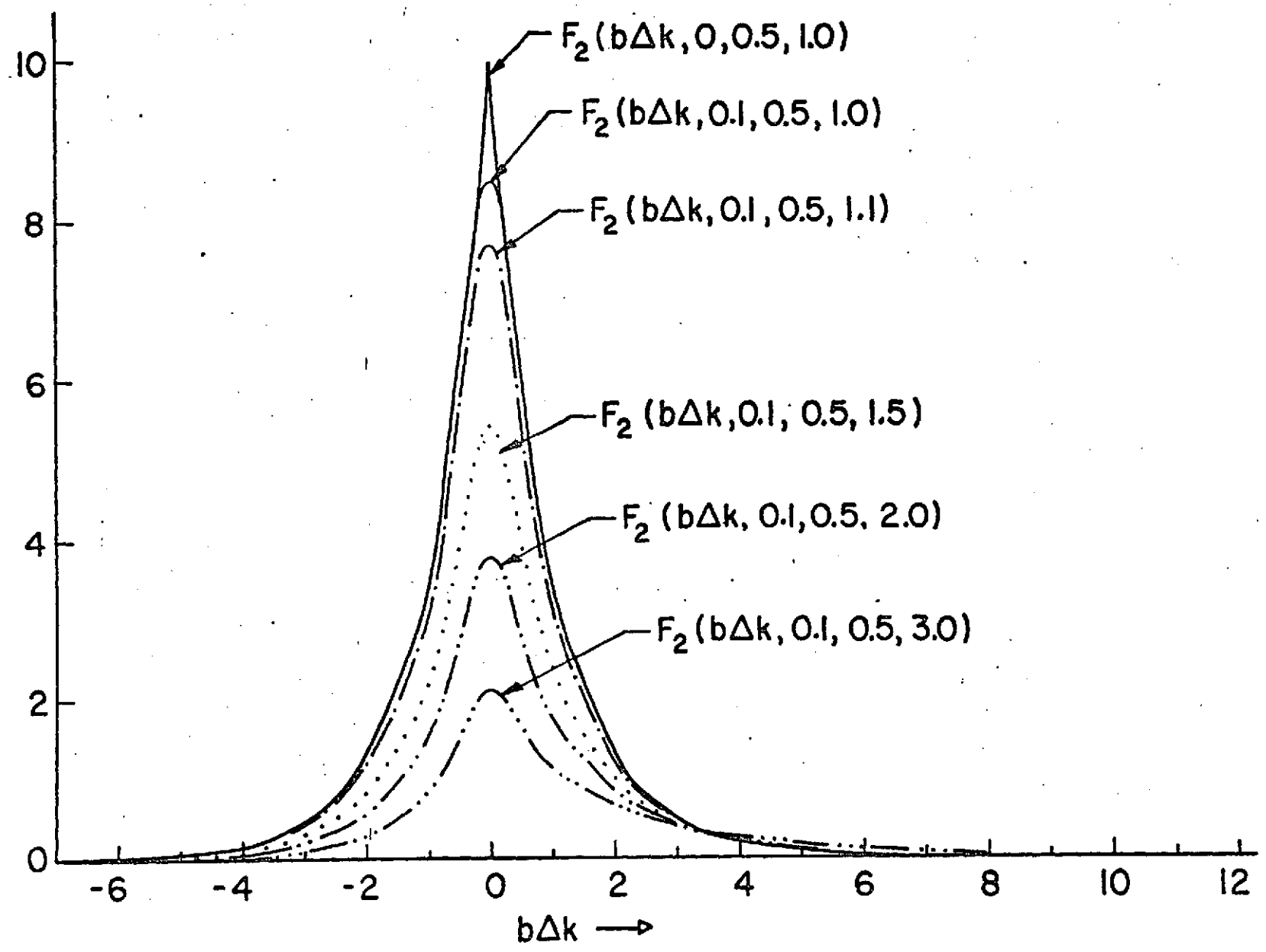


Fig. 2-- F_2 vs. $b\Delta k$ for $b/L \leq 0.1$; $f/L = 0.5$; and $k''/k' = 1.0, 1.1, 1.5, 2.0, \text{ and } 3.0$.

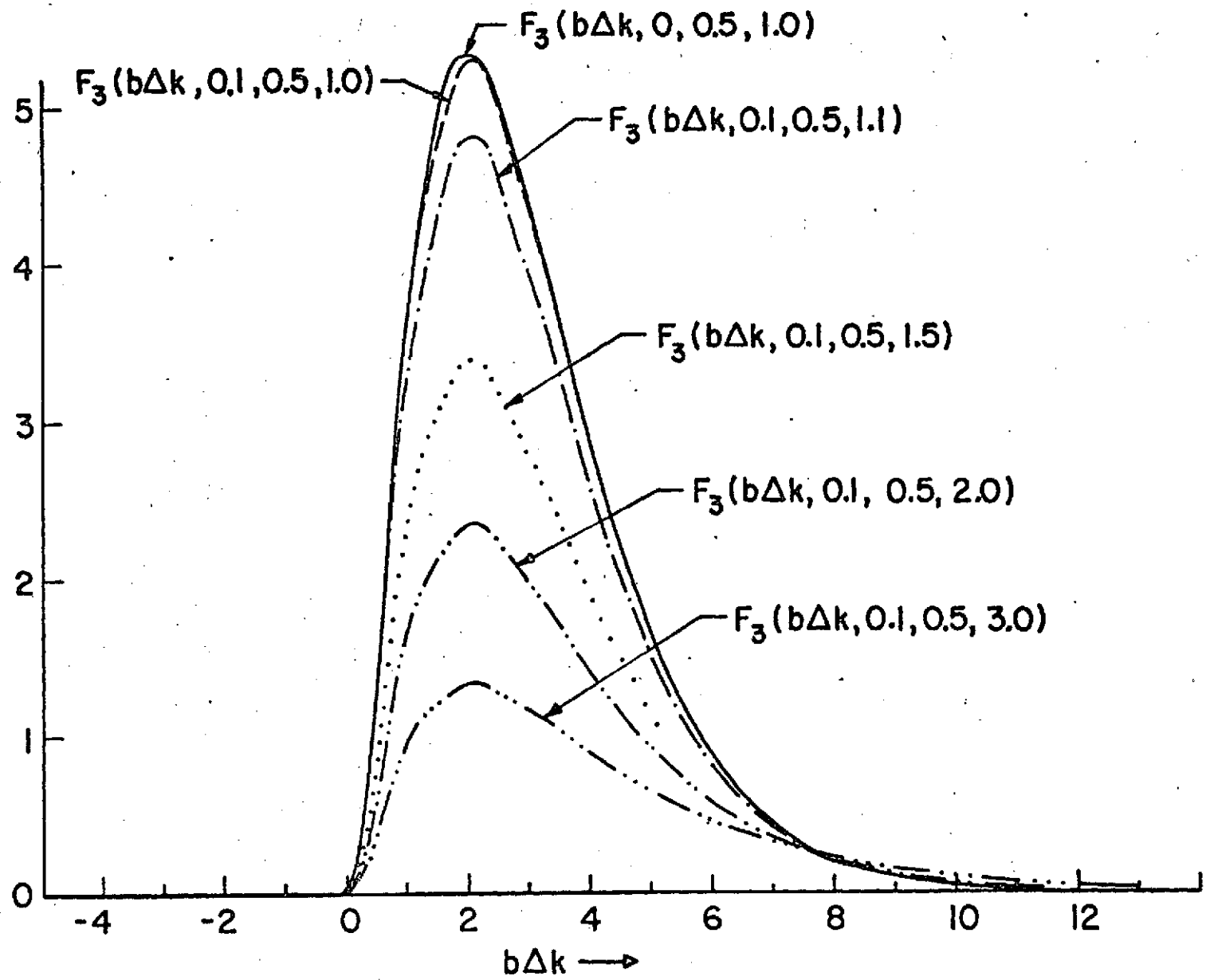


Fig. 3-- F_3 vs. $b\Delta k$ for $b/L \leq 0.1$; $f/L = 0.5$; and $k''/k' = 1.0$, 1.1 , 1.5 , 2.0 , and 3.0 .

TABLE I

 F_j vs. $b\Delta k$ for tight focusing cases

F_j	Peak Value	Value of $b\Delta k$ at peak	Range of $b\Delta k$ for which $F_j \geq 50\%$ of peak	Range of $b\Delta k$ for which $F_j \geq 10\%$ of peak	Range of $b\Delta k$ for which $F_j \geq 0.1\%$ of peak
$F_1(b\Delta k, 0, 0.5, 1)$	5.3	- 2.0	- 4.1 to - 0.8	- 6.7 to - 0.3	- 12.5 to - 0.1
$F_1(b\Delta k, 0.1, 0.5, 1)$	5.4	- 2.1	- 4.1 to - 0.8	- 6.7 to - 0.3	- 12.5 to + 0.1
$F_1(b\Delta k, 0.1, 0.75, 1)$	5.5	- 2.0	- 4.1 to - 0.9	- 6.7 to - 0.3	- 12.5 to + 0.6
$F_1(b\Delta k, 0.1, 0.85, 1)$	5.4	- 2.2	- 4.1 to - 0.9	- 6.7 to - 0.3	- 12.4 to + 1.9
$F_2(b\Delta k, 0, 0.5, 1)$	9.9	0.0	- 0.7 to + 0.7	- 2.3 to + 2.3	- 6.9 to + 6.9
$F_2(b\Delta k, 0.1, 0.5, 1)$	8.5	0.0	- 0.8 to + 0.8	- 2.4 to + 2.4	- 7.0 to + 7.0
$F_2(b\Delta k, 0.1, 0.5, 1.1)$	7.7	0.0	- 0.8 to + 0.8	- 2.4 to + 2.4	- 7.0 to + 7.0
$F_2(b\Delta k, 0.1, 0.5, 1.5)$	5.4	0.0	- 0.8 to + 0.9	- 2.4 to + 2.7	- 7.0 to + 8.7
$F_2(b\Delta k, 0.1, 0.5, 2)$	3.8	0.0	- 0.8 to + 0.9	- 2.4 to + 3.3	- 7.0 to + 11.4
$F_2(b\Delta k, 0.1, 0.5, 3)$	2.1	0.0	- 0.8 to + 1.0	- 2.4 to + 4.6	- 7.0 to + 16.9
$F_3(b\Delta k, 0, 0.5, 1)$	5.3	+ 2.0	+ 0.8 to + 4.1	+ 0.3 to + 6.7	+ 0.1 to + 12.5
$F_3(b\Delta k, 0.1, 0.5, 1)$	5.3	+ 2.1	+ 0.8 to + 4.1	+ 0.3 to + 6.7	+ 0.1 to + 12.6
$F_3(b\Delta k, 0.1, 0.5, 1.1)$	4.8	+ 2.1	+ 0.8 to + 4.1	+ 0.3 to + 6.7	+ 0.1 to + 12.6
$F_3(b\Delta k, 0.1, 0.5, 1.5)$	3.4	+ 2.1	+ 0.8 to + 4.2	+ 0.3 to + 7.1	+ 0.1 to + 13.8
$F_3(b\Delta k, 0.1, 0.5, 2)$	2.3	+ 2.1	+ 0.7 to + 4.4	+ 0.3 to + 7.8	+ 0.1 to + 16.3
$F_3(b\Delta k, 0.1, 0.5, 3)$	1.4	+ 2.1	+ 0.7 to + 4.9	+ 0.3 to + 9.3	+ 0.1 to + 22.0

The value of k''/k' is irrelevant to the behavior of the F_j in the plane wave case. The peak of this sinc^2 function is offset from zero by $\Delta k = -4/b$ for F_1 and by $\Delta k = 4/b$ for F_3 , while for F_2 the peak is always at zero.

The complete evolution of the form of the F_j from the tight focusing limit to the plane wave limit is demonstrated in Figs. 4 and 5 for the case of F_1 . Families of curves of F_1 vs. $b\Delta k$ for various locations of the focus (various values of f/L) are plotted in Figs. 6, 7, 8, 9, and 10, where each figure corresponds to a different, constant value of b/L . Figure 6 illustrates that, for tight focusing, F_j vs. $b\Delta k$ is relatively unchanged as long as the fundamental beam waist region is entirely contained within the cell. Figure 10 illustrates that, for b much larger than L , F_j vs. $b\Delta k$ is relatively unchanged as long as the cell is located close to the beam waist location. Figures 7, 8, and 9 show the more complicated behavior of the intermediate cases. In every case, however, when the beam waist location is far outside of the cell, the location of the peak of the F_j lies very near to $b\Delta k = 0$.

The dependence of the mode structure of the generated radiation upon $b\Delta k$ may be determined by monitoring $|E_{\perp}(\vec{R})|^2$ as a function of the transverse coordinate R for each value of $b\Delta k$. For the processes $\omega_1 + \omega_2 - \omega_3 \rightarrow \omega_4$ and $\omega_1 - \omega_2 - \omega_3 \rightarrow \omega_4$, when $k''/k' \neq 1$, the far-field intensity distribution evolves from a nearly Gaussian shape for $b\Delta k \leq 0$, to a circularly symmetric ring pattern as $b\Delta k$ becomes large and positive. This nearly Gaussian shape is in close agreement with the far-field intensity distribution which would arise from a lowest order Gaussian mode with the same

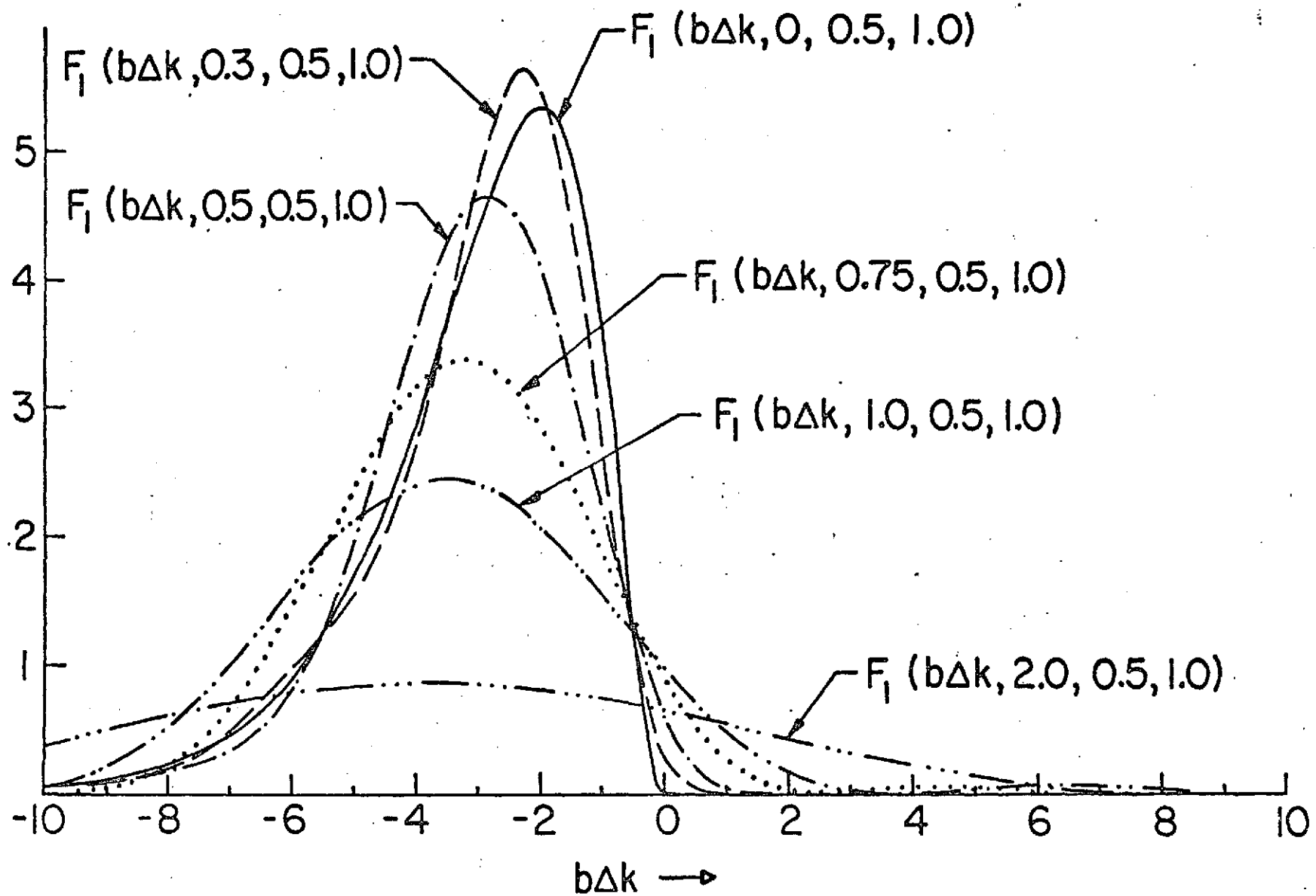


Fig. 4-- F_1 vs. $b\Delta k$ for $f/L = 0.5$ and $b/L = 0, 0.3, 0.5, 0.75, 1.0, \text{ and } 2.0$.

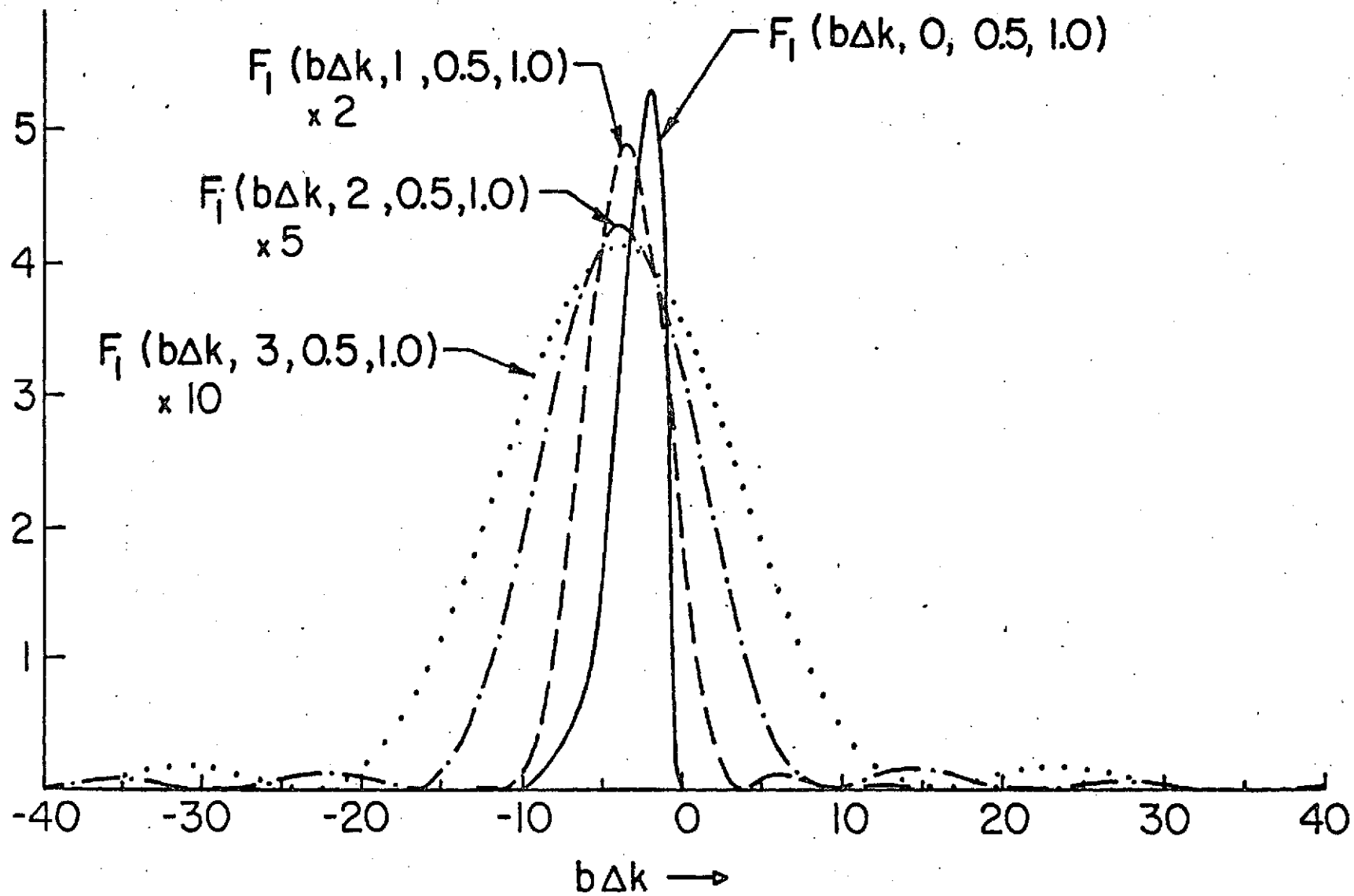


Fig. 5-- F_1 vs. $b\Delta k$ for $f/L = 0.5$ and $b/L = 0, 1, 2,$ and 3 .

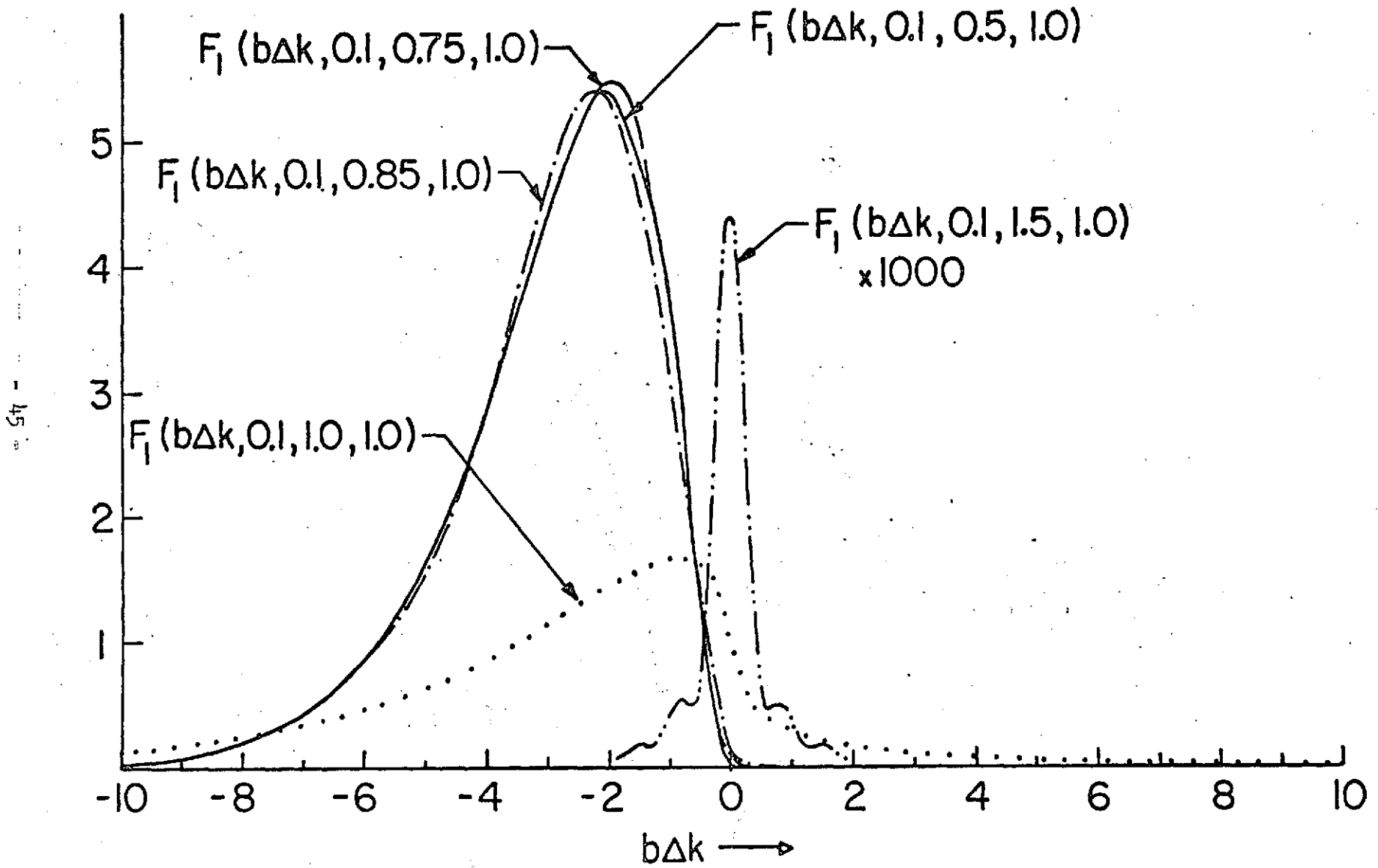


Fig. 6-- F_1 vs. $b\Delta k$ for $b/L = 0.1$ and $f/L = 0.5, 0.75, 0.85, 1.0, \text{ and } 1.5$.

- 94 -

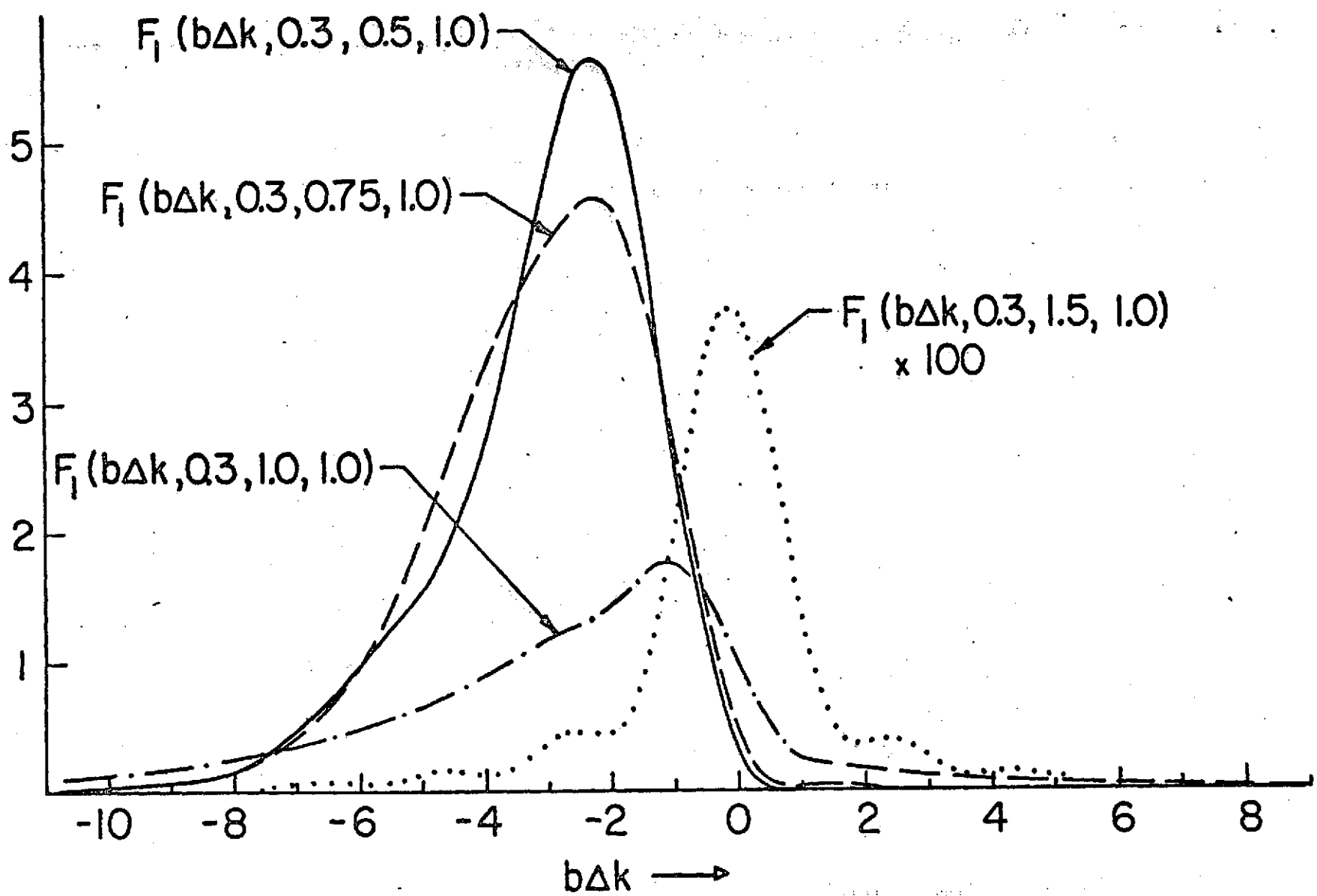


Fig. 7-- F_1 vs. $b\Delta k$ for $b/L = 0.3$ and $f/L = 0.5, 0.75, 1.0, \text{ and } 1.5$.

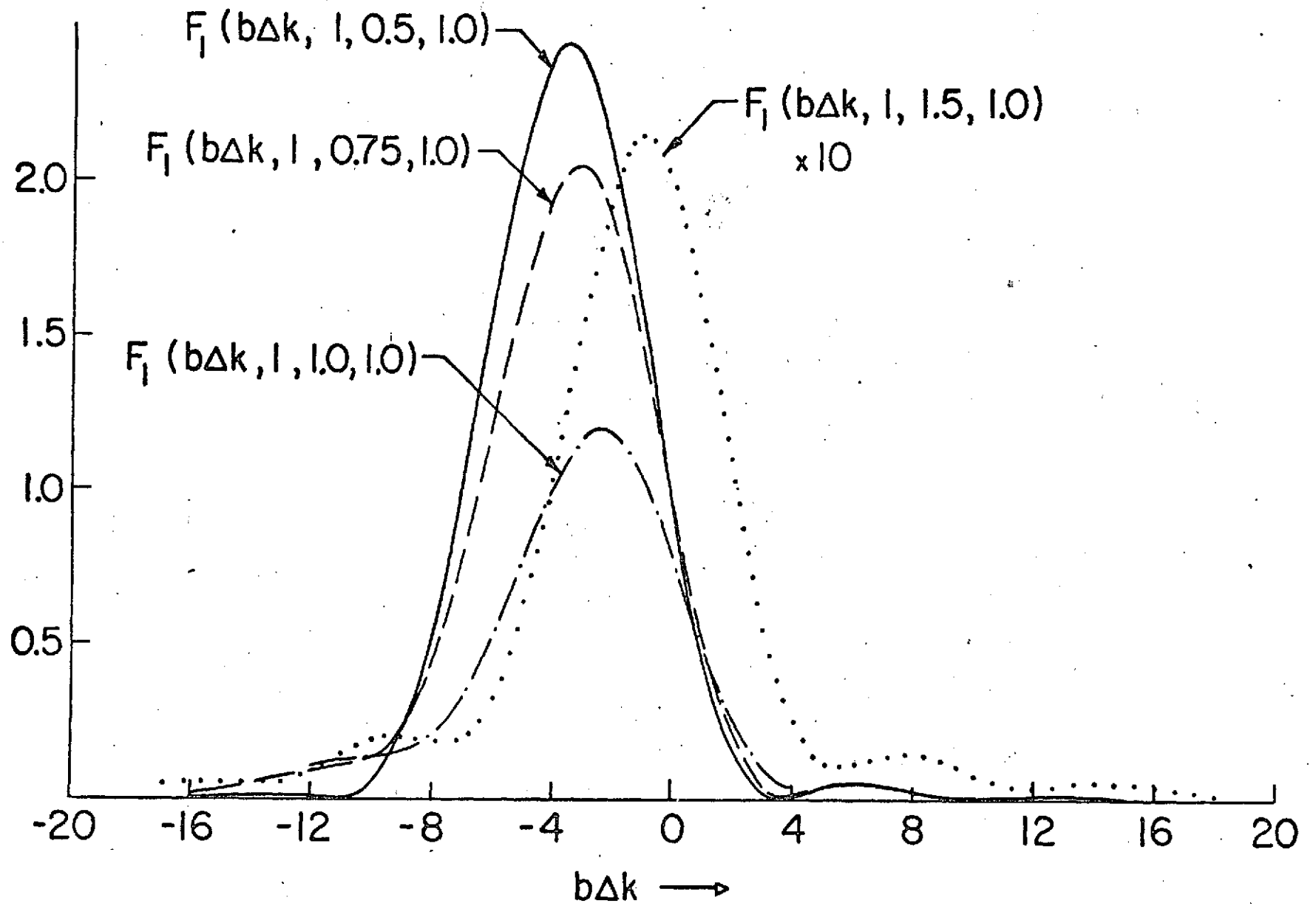


Fig. 8-- F_1 vs. $b\Delta k$ for $b/L = 1$ and $f/L = 0.5, 0.75, 1.0,$ and 1.5 .

- 87 -

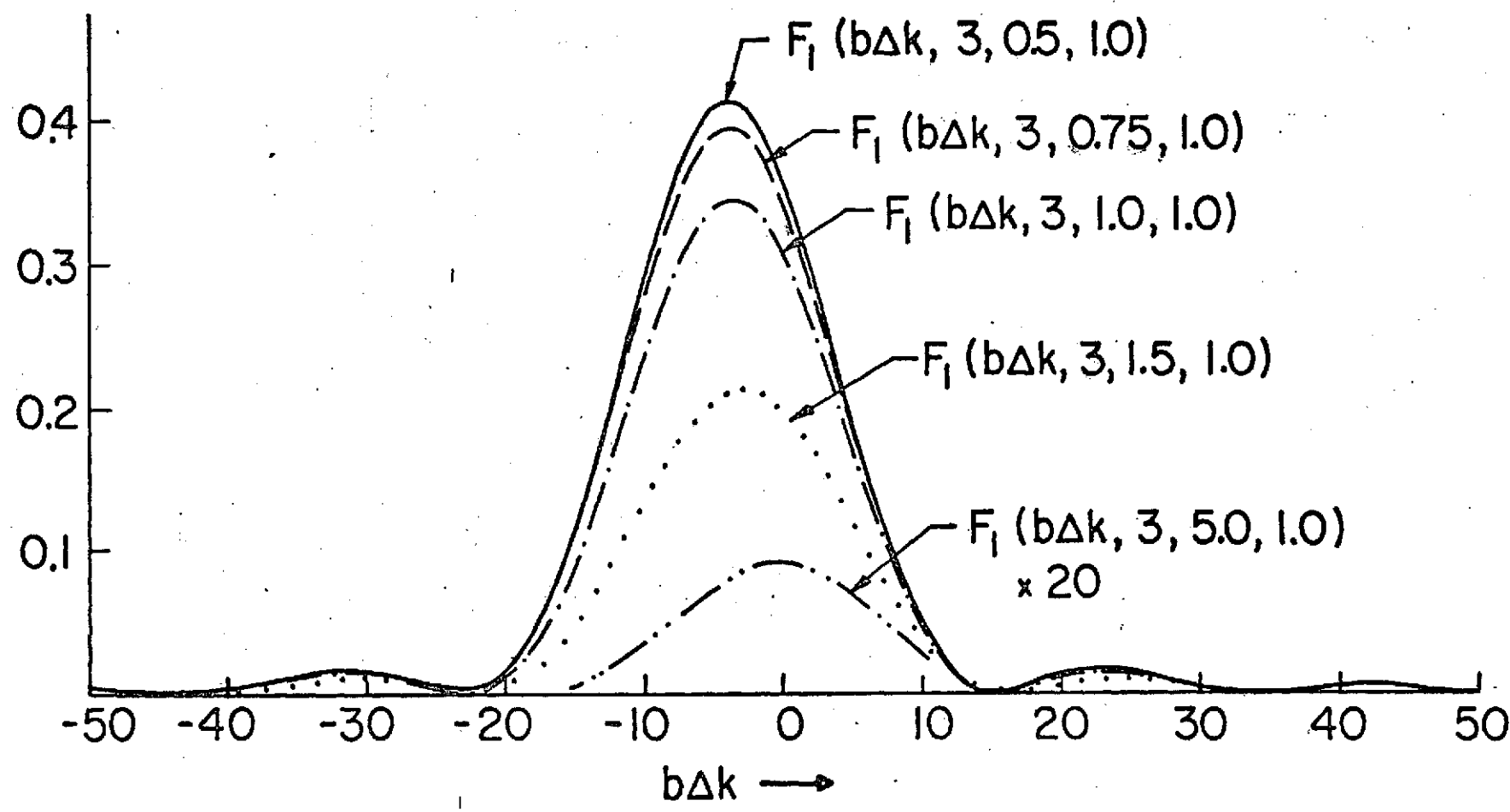


Fig. 9-- F_1 vs. $b\Delta k$ for $b/L = 3$ and $f/L = 0.5, 0.75, 1.0, 1.5,$ and 5.0 .

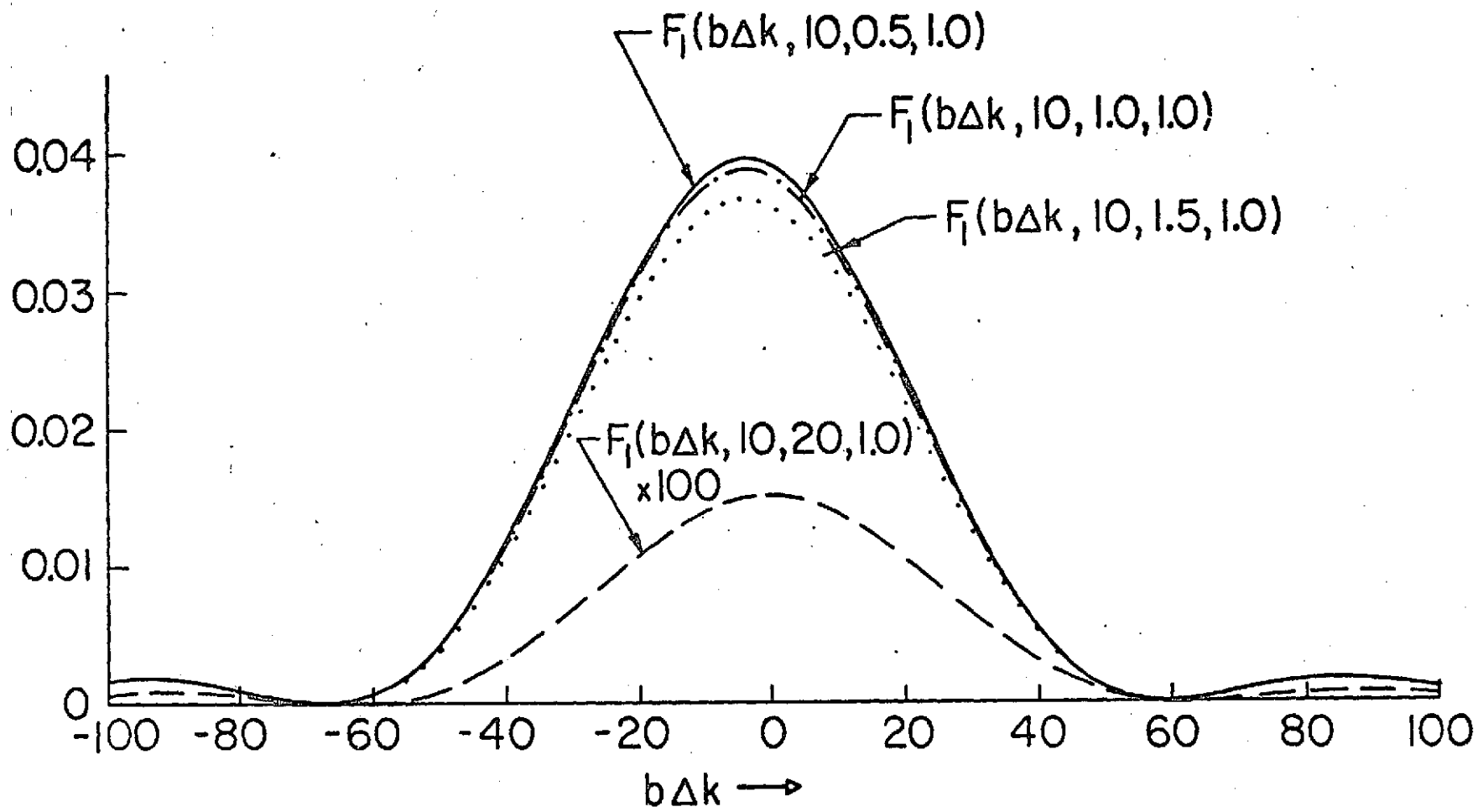


Fig. 10-- F_1 vs. $b\Delta k$ for $b/L = 10$ and $f/L = 0.5, 1.0, 1.5,$ and 2.0 .

wavelength as the generated radiation and with the same confocal parameter and waist location as the fundamental beams. The circularly symmetric ring pattern is of the type which has been observed by Terhune¹⁹ and others for anti-Stokes radiation produced by three-wave mixing. The results of this section thus indicate that this ring pattern will appear only when $b\Delta k$ is positive. A typical evolution of the far-field pattern as Δk is changed is presented in Fig. 11 for the process $\omega_1 + \omega_2 - \omega_3 \rightarrow \omega_4$ with $k''/k' = 3$.

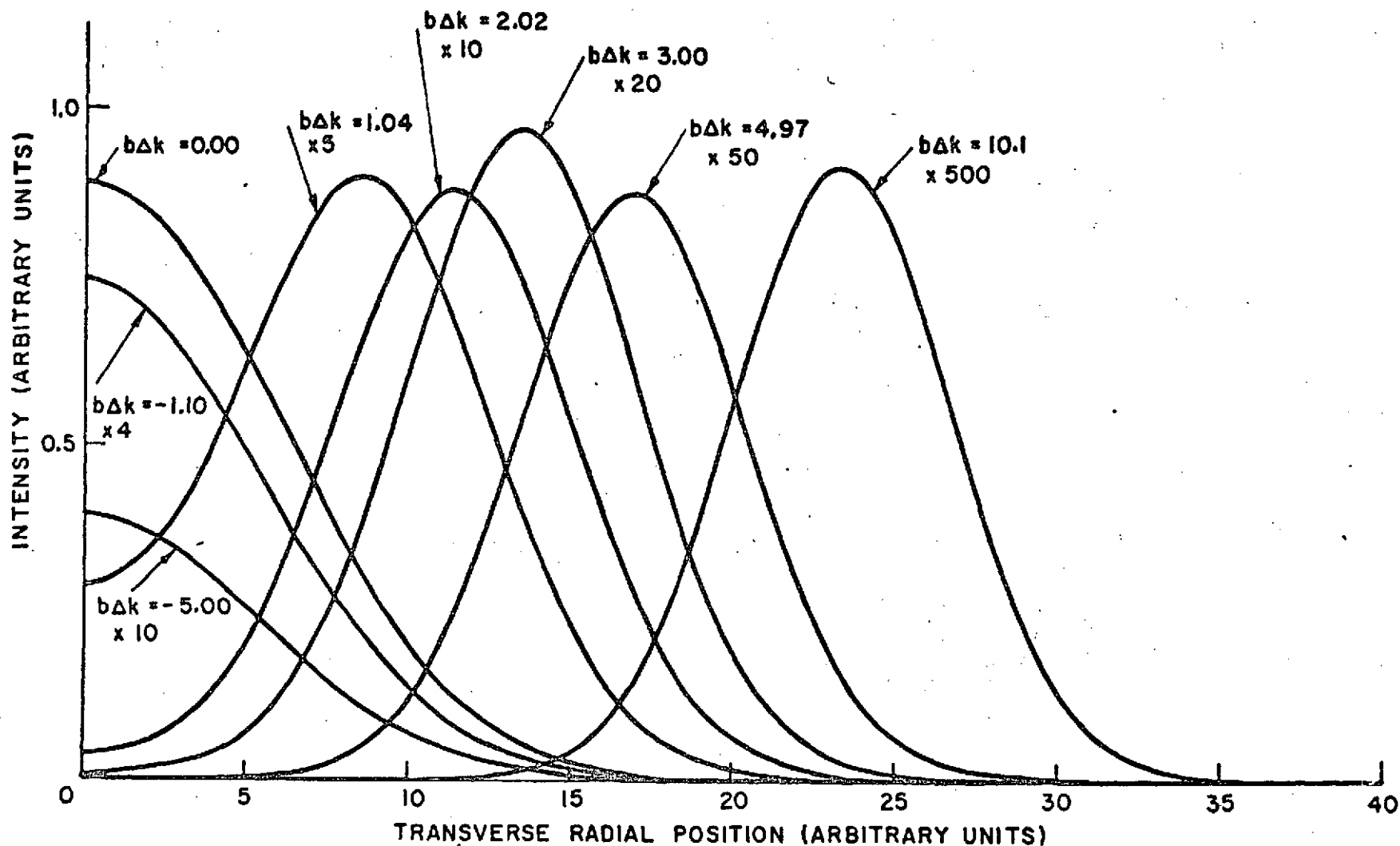


Fig. 11--Far-field intensity distribution for several values of $b\Delta k$ for the process $\omega_1 + \omega_2 - \omega_3 \rightarrow \omega_4$ with $k''/k' = 3.0$. The distribution in each case is calculated at the position of the output window of a cell with $b/L = 0.1$ and $f/L = 0.5$.

IV. A PHYSICAL BASIS FOR THE BEHAVIOR OF THE F_j

Several aspects of the behavior of the F_j , including the optimum values of $b\Delta k$ and the invariance with respect to the exact location of the focus in the tight focusing case, may be explained by a simple model which takes into account the additional phase shift caused by focusing.

From Eqs. (2) and (6), it can be seen that the amplitude of the driving polarization strongly peaks in the region of the fundamental beam waists. A region of significant generation may somewhat arbitrarily be defined as bounded by the z values at which the driving polarization falls to 10% of its peak value. In the case of tight focusing, when b is much less than L and the fundamental beam waist region is located entirely within the cell, the boundaries of the generating region are located at $\mathcal{E} = -2$ and $\mathcal{E} = +2$ (or $z = f - b$ and $z = f + b$). In the case of loose focusing, when b is much larger than L , the boundaries are located at the input and output windows of the cell.

From Eq. (2), it can be seen from the term

$$(1 + i\mathcal{E})^{-1} = (1 + \mathcal{E}^2)^{-\frac{1}{2}} \exp(-i \tan^{-1} \mathcal{E})$$

that a focused lowest order Gaussian beam undergoes a shift in phase given by $\tan^{-1} \mathcal{E}$ as it propagates through the waist region. The driving

polarization given by Eq. (6) then experiences a phase shift of $3 \tan^{-1} \epsilon$ for $\omega_1 + \omega_2 + \omega_3 \rightarrow \omega_4$, $\tan^{-1} \epsilon$ for $\omega_1 + \omega_2 - \omega_3 \rightarrow \omega_4$, and $-\tan^{-1} \epsilon$ for $\omega_1 - \omega_2 - \omega_3 \rightarrow \omega_4$. If it is assumed that the optimum conversion efficiency occurs when the generated radiation is nearly a lowest order Gaussian mode with the same confocal parameter as the fundamental beams, then the generated radiation may be considered to experience a phase shift of $\tan^{-1} \epsilon$. Thus a slip in phase between the driving polarization and the generated radiation of $2 \tan^{-1} \epsilon$ for $\omega_1 + \omega_2 + \omega_3 \rightarrow \omega_4$ and of $-2 \tan^{-1} \epsilon$ for $\omega_1 - \omega_2 - \omega_3 \rightarrow \omega_4$ occurs, while no slip in phase occurs for $\omega_1 + \omega_2 - \omega_3 \rightarrow \omega_4$. This slip in phase causes destructive interference between radiation generated in different portions of the generating region.

The slip in phase due to focusing may be compensated to some degree by the wave vector mismatch, Δk , introduced by the dispersion of the nonlinear medium. The optimum value of Δk , Δk_{opt} , is that value which exactly cancels the total slip in phase which occurs as the generating region is traversed.

In the case of tight focusing, when the entire generating region is contained within the cell, this requirement yields

$$\Delta k_{\text{opt}} \cong \begin{cases} -2.2/b & \text{for } \omega_1 + \omega_2 + \omega_3 \rightarrow \omega_4 \\ 0 & \text{for } \omega_1 + \omega_2 - \omega_3 \rightarrow \omega_4 \\ +2.2/b & \text{for } \omega_1 - \omega_2 - \omega_3 \rightarrow \omega_4 \end{cases}, \quad (37)$$

in good agreement with the exact results. Since significant generation occurs only in the generating region, it follows that this behavior should be

independent of the exact location of the focus so long as the entire generating region is contained within the cell.

In the case of loose focusing, when the entire cell is located in the beam waist, these arguments yield

$$\Delta k_{\text{opt}} = \begin{cases} -\frac{4}{b} & \text{for } \omega_1 + \omega_2 + \omega_3 \rightarrow \omega_4 \\ 0 & \text{for } \omega_1 + \omega_2 - \omega_3 \rightarrow \omega_4 \\ \frac{4}{b} & \text{for } \omega_1 - \omega_2 - \omega_3 \rightarrow \omega_4 \end{cases}, \quad (38)$$

again in good agreement with the exact results.

V. OPTIMIZATION OF THE TIGHT FOCUSING CASE

In this section, procedures for the optimization of the total generated power are developed for the case of tight focusing ($b/L \leq 0.1$) with the fundamental beam waist region entirely contained within the cell. If limiting processes¹ such as pump depletion, absorption, breakdown, saturation, thermal defocusing, and the quadratic Kerr effect are neglected, then the total generated power at ω_4 is always given by Eq. (31) and thus obeys the proportionality relation

$$P_4 \propto P_1 P_2 P_3 N^2 \chi^2 F_j(b\Delta k, b/L, f/L, k''/k') \quad (39)$$

The parameters $P_1 P_2 P_3$, χ , and k''/k' are considered to be constant and thus the optimization procedure reduces to maximizing the quantity $N^2 F_j(b\Delta k, b/L, f/L, k''/k')$ by varying the parameters N , $b\Delta k$, b/L , and f/L .

When N is a parameter which is independent of $b\Delta k$, b/L , and f/L , the optimization procedure further simplifies to increasing N to the highest possible value while independently maximizing F_j . By the results of Section III, the maximization conditions for the F_j under these

tight focusing conditions are then simply to set $b\Delta k$ to $b\Delta k_{opt}$ given by

$$b\Delta k_{opt} = \begin{cases} -2 & \text{for } \omega_1 + \omega_2 + \omega_3 \rightarrow \omega_4 \\ 0 & \text{for } \omega_1 + \omega_2 - \omega_3 \rightarrow \omega_4 \\ +2 & \text{for } \omega_1 - \omega_2 - \omega_3 \rightarrow \omega_4 \end{cases} \quad (40)$$

regardless of the exact values of b/L and f/L (so long as $b/L \leq 0.1$ and $b \leq f \leq L - b$).

The parameter $b\Delta k$ may be adjusted to its optimum value by means of altering b or by altering Δk . The value of b may be straightforwardly altered by varying the tightness of focus, but in order for the tight focusing approximation of this section to remain valid, b/L must remain less than 0.1. In order to make Δk a parameter which is independent of N , another medium with negligible nonlinearity but appreciable dispersion may be mixed with the nonlinear medium.¹ Δk could then be controlled by varying the concentration of the added medium. The process $\omega_1 + \omega_2 - \omega_3 \rightarrow \omega_4$ is unique in that the optimum value of b is always zero, regardless of the value of Δk . It should be noted that the procedure of optimizing by adjusting b is valid only if the nonlinear medium can tolerate the high power densities introduced by very tight focusing. If this is not possible, the best compromise is to reduce b to the smallest permissible value and then to adjust Δk to reach $b\Delta k_{opt}$.

The value of F_j is severely reduced if $b\Delta k$ deviates from its optimum value. The tolerances on the value of $b\Delta k$ which correspond to F_j maintaining at least 50%, 10%, and 0.1% of its peak value are given in Table I

of Section III. It is particularly important to note that the process $\omega_1 + \omega_2 + \omega_3 \rightarrow \omega_4$ requires that $b\Delta k$ be non-zero and positive while the process $\omega_1 - \omega_2 - \omega_3 \rightarrow \omega_4$ requires that $b\Delta k$ be non-zero and negative. The generated total power at ω_4 under these optimized conditions is given by Eq. (29) with F_j set to its peak value from Table I.

Different optimization procedures are required when N is a parameter which is not independent of $b\Delta k$. One particularly important case occurs when Δk is constrained to be proportional to N while b is constrained to be constant and N is a free parameter. In this case, the quantity which must be maximized in the optimization procedure is $\Delta k^2 F_j(b\Delta k, b/L, f/L, k''/k')$. This quantity is not dimensionless, and depends on the absolute value of b . Therefore it is appropriate to define the dimensionless quantity

$$G_j(b\Delta k, b/L, f/L, k''/k') = (\Delta k b)^2 F_j(b\Delta k, b/L, f/L, k''/k') \quad , \quad (41)$$

and to realize that the quantity which must be maximized is then

$$(1/b)^2 G_j(b\Delta k, b/L, f/L, k''/k') \quad .$$

G_1 is plotted for $b/L = 0$ and $b/L = 1$ with $f/L = 0.5, 0.75,$ and 0.85 in Fig. 12. The location and magnitude of the peaks of G_j are summarized in Table II. Here it is apparent that, as in the case of the F_j , the value of b/L in the G_j may be to a good approximation be replaced by zero for b/L less than 0.1. In addition, for tight focusing, the G_j are independent of the value of f/L as long as the entire input beam waist region is contained within the cell. G_2 is plotted for $f/L = 0.5,$

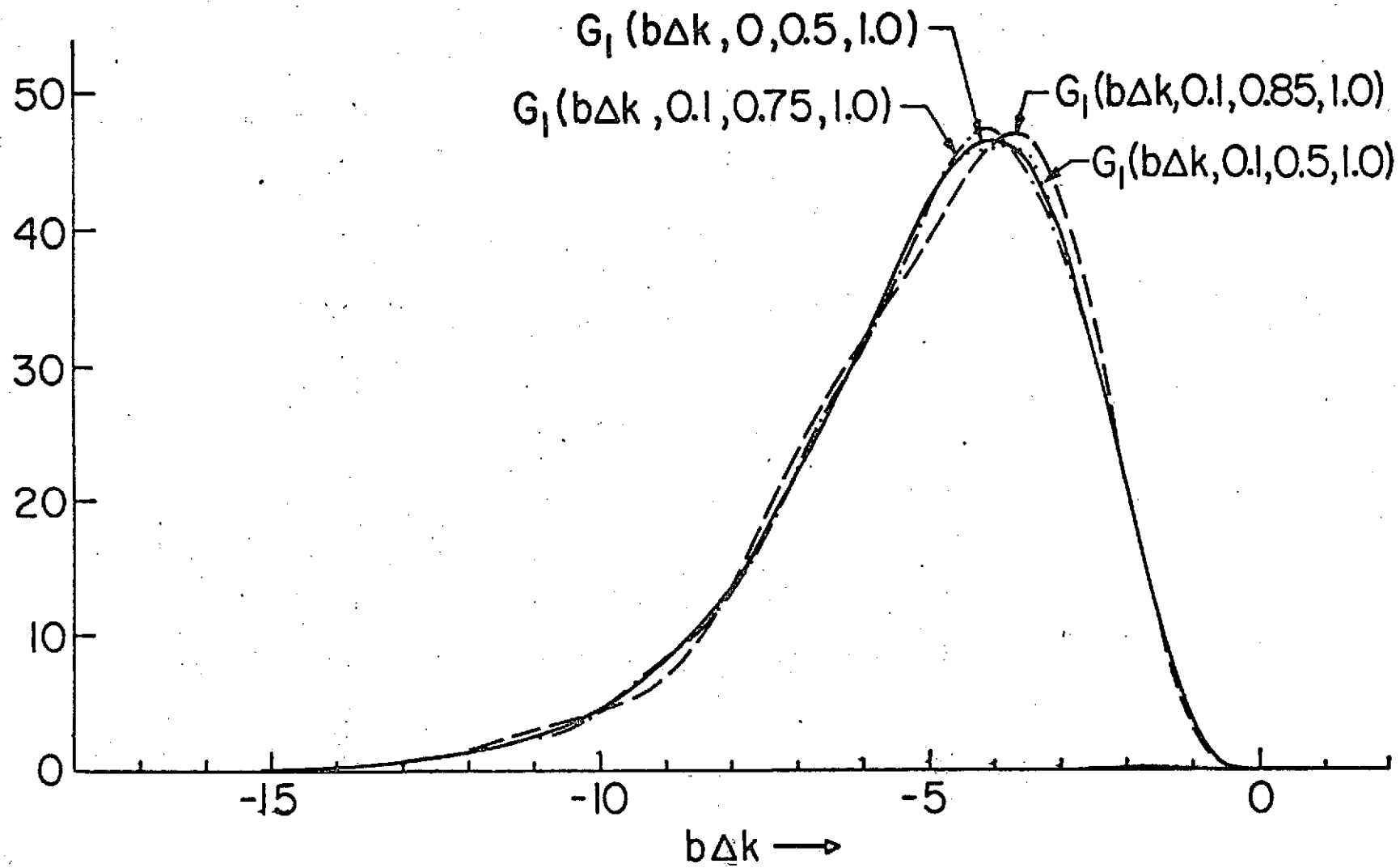


Fig. 12-- G_1 vs. $b\Delta k$ for $b/L \leq 0.1$ and $f/L = 0.5, 0.75,$ and 0.85 .

TABLE II

Behavior of $G_j(b\Delta k, b/L, f/L, k''/k')$ for tight focusing cases

G_j	Peak Value(s)	Value of $b\Delta k$ at Peak
$G_1(b\Delta k, 0, 0.5, 1)$	46.3	- 4.0
$G_1(b\Delta k, 0.03, 0.5, 1)$	46.3	- 4.0
$G_1(b\Delta k, 0.1, 0.5, 1)$	45.9	- 3.8
$G_1(b\Delta k, 0.1, 0.75, 1)$	47.2	- 4.1
$G_1(b\Delta k, 0.1, 0.85, 1)$	46.8	- 3.7
$G_2(b\Delta k, 0, 0.5, 1)$	53.4 53.4	- 2.0 + 2.0
$G_2(b\Delta k, 0.1, 0.5, 1)$	53.4 53.4	- 1.8 + 1.8
$G_2(b\Delta k, 0.1, 0.5, 1.1)$	48.5 49.0	- 1.8 + 1.8
$G_2(b\Delta k, 0.1, 0.5, 1.5)$	34.2 40.6	- 1.8 + 2.6
$G_2(b\Delta k, 0.1, 0.5, 2.0)$	23.8 40.3	- 1.8 + 3.0
$G_2(b\Delta k, 0.1, 0.5, 3.0)$	13.3 45.0	- 1.8 + 5.0
$G_3(b\Delta k, 0, 0.5, 1)$	46.3	+ 4.0
$G_3(b\Delta k, 0.1, 0.5, 1)$	45.7	3.8
$G_3(b\Delta k, 0.1, 0.5, 1.1)$	41.5	3.8
$G_3(b\Delta k, 0.1, 0.5, 1.5)$	30.8	4.4
$G_3(b\Delta k, 0.1, 0.5, 2.0)$	23.6	4.6
$G_3(b\Delta k, 0.1, 0.5, 3.0)$	16.6	5.8

$b/L = 0.1$ in Figs. 13 and 14. G_3 is plotted for $f/L = 0.5$, $b/L = 0.1$ in Fig. 15.

Since N is the only free parameter, the optimization procedure is to adjust $b\Delta k$ to maximize G_j by adjusting N . Let $(b\Delta k)_{opt}$ be the value of $b\Delta k$ as given in Table II which corresponds to the peak of G_j . Define the coefficient of proportionality, α , by the relation $\Delta k = \alpha N$. Then the optimization procedure reduces to adjusting N to the value

$$N_{opt} = (b\Delta k)_{opt} / \alpha b$$

From Eqs. (29) and (41), the total generated power in this optimized case is

$$P_4 = (6.318 \times 10^{-4}) \frac{k_0^4 k_1 k_2 k_3}{k_4^2 k'} \frac{\chi^2 P_1 P_2 P_3 G_j}{\alpha^2 b^2} \quad (42)$$

where G_j is given its peak value from Table II.

It may be noted that in order to reach this optimized condition, α must be negative for the process $\omega_1 + \omega_2 + \omega_3 \rightarrow \omega_4$, while α must be positive for the process $\omega_1 - \omega_2 - \omega_3 \rightarrow \omega_4$. The process $\omega_1 + \omega_2 - \omega_3 \rightarrow \omega_4$ is unique in that G_2 possesses peaks for positive and negative $b\Delta k$ and thus α may be either negative or positive.

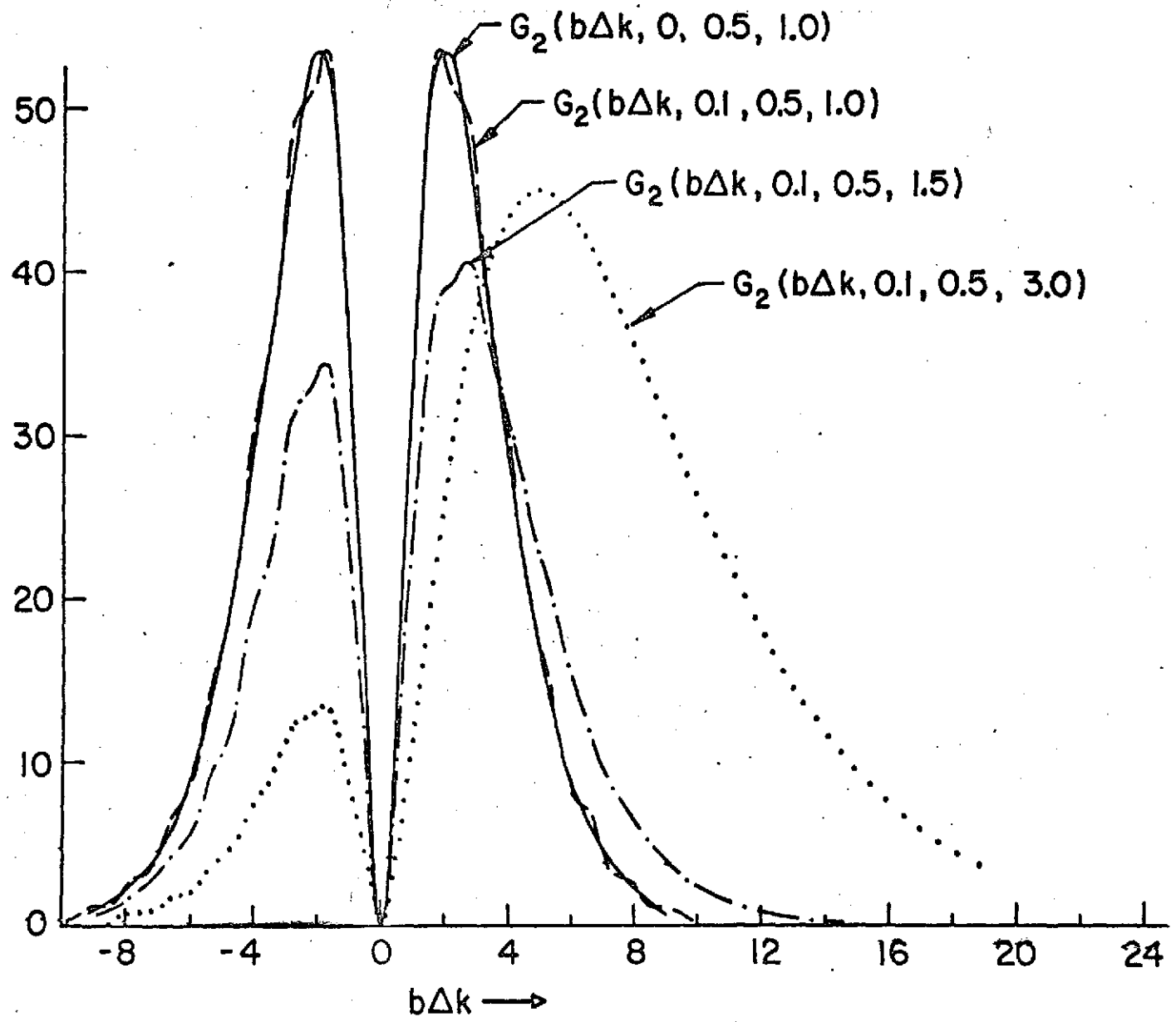


Fig. 13-- G_2 vs. $b\Delta k$ for $b/L \leq 0.1$; $f/L = 0.5$; and $k''/k' = 1.0, 1.5,$ and 3.0 .

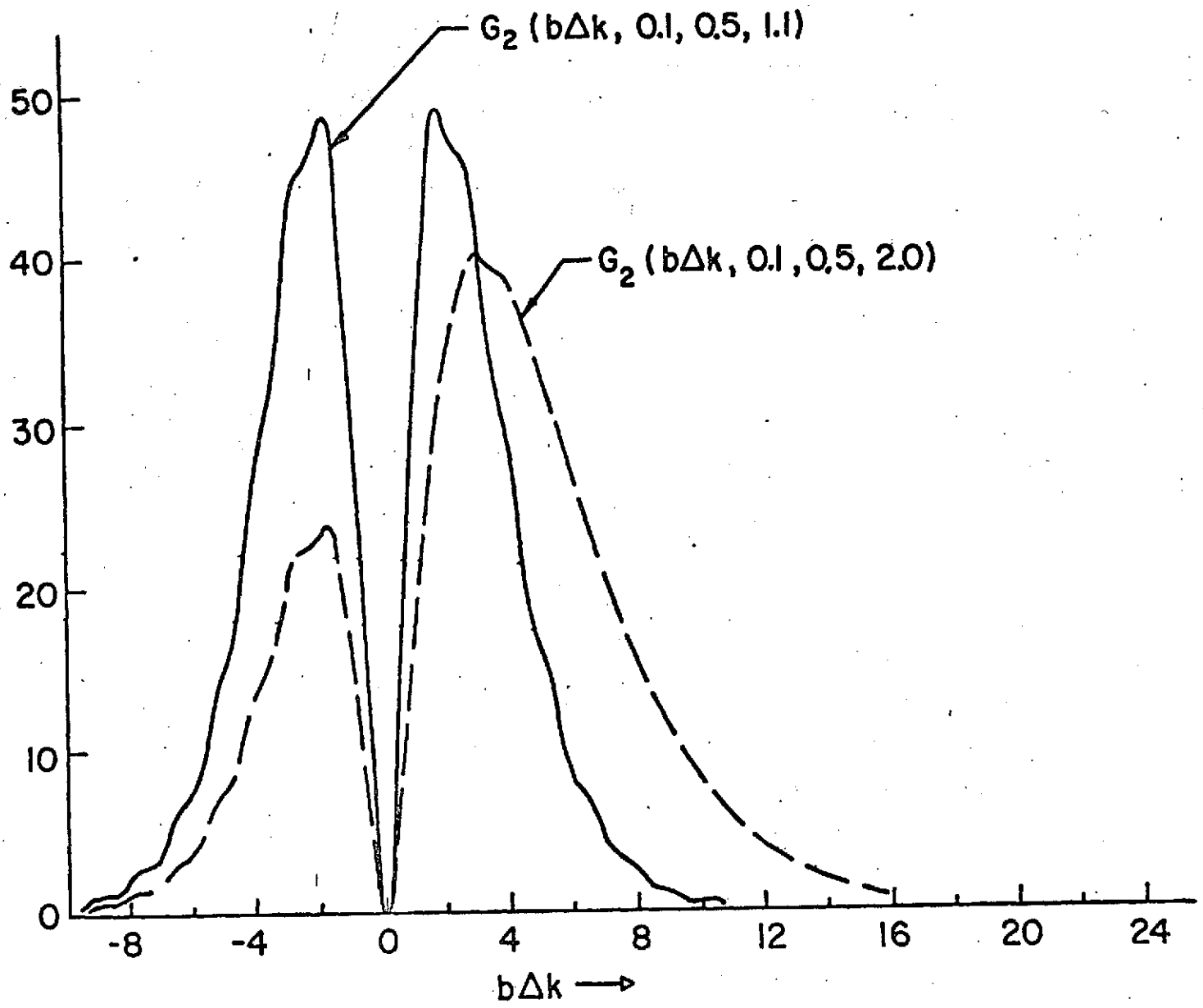


Fig. 14-- G_2 vs. $b\Delta k$ for $b/L \leq 0.1$; $f/L = 0.5$; and $k''/k' = 1.1$ and 2.0 .

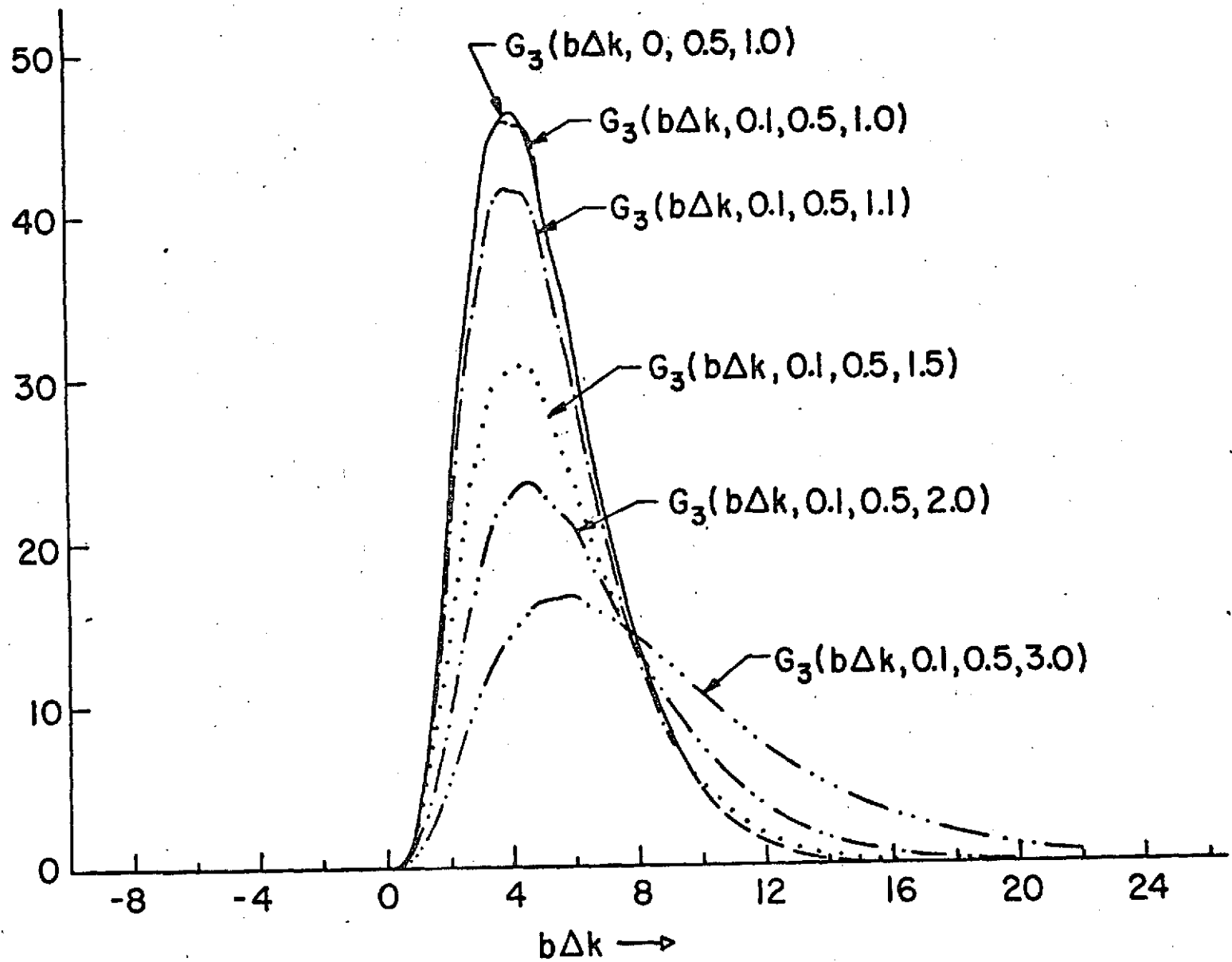


Fig. 15-- G_3 vs. $b\Delta k$ for $b/L \leq 0.1$; $f/L = 0.5$; and $k''/k' = 1.0, 1.1, 1.5, 2.0, \text{ and } 3.0$.

VI. EXPERIMENTAL RESULTS

An experiment has been conducted which verifies the theory of this paper for the process $\omega_1 + \omega_1 + \omega_1 \rightarrow 3\omega_1$ (third harmonic generation) in the case of very tight focusing near the center of the cell. In these experiments the nonlinear medium was Xe gas, the fundamental beam had a wavelength of 3547 \AA , and the generated radiation had a wavelength of 1182 \AA . For this process, Xe possesses both a high nonlinear susceptibility and the proper dispersion characteristics to produce a negative value for Δk .

The experimental set-up was identical with that of Kung, et al.,⁶ except that the 3547 \AA beam was passed through a lens-diamond pinhole-shearing aperture spatial filter in order to produce a very high quality diffraction limited beam with well known parameters.

In this experiment, approximately 0.1% of the 3547 \AA radiation was converted to 1182 \AA radiation. The fundamental beam was focused at the center of the cell and b/L was 0.025. Figure 16 shows the relative power output at 1182 \AA vs. Xe pressure with no Ar in the cell. The agreement of the triangular data points to the theoretical function $G_1(b\Delta k, 0, 0.5, 1)$ is excellent. The departure of the circular data points from theory is caused by the multimode character of the fundamental beam which results from an incorrect shearing aperture diameter. The process of fitting G_1 to the data yields the coefficient of proportionality between Δk and the

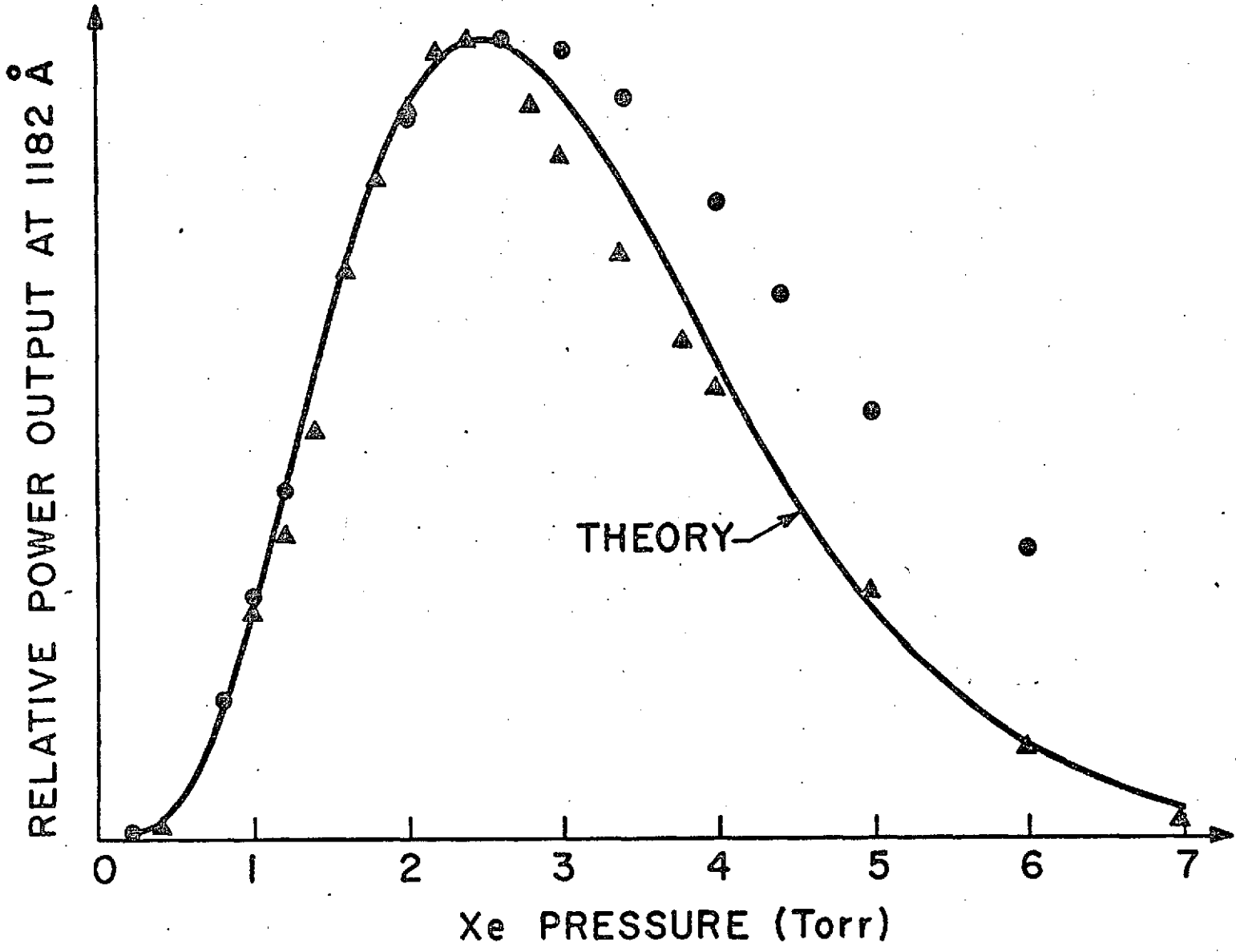


Fig. 16--Relative output at 1182 Å vs. Xe pressure. (The triangular points represent data from a run in which the shearing aperture was set to the proper diameter. The circular points represent data from a run in which the shearing aperture was open too far. The solid curve represents the best fit to the function $G_1(b_{4\lambda}, 0, 0.5, 1)$ to the triangular points.)

atomic number density of the nonlinear medium, and thus provides an alternative method of determining the dispersion between the fundamental and generated wavelengths. The fit in Fig. 16 yielded $\Delta k = (-5.99 \times 10^{-17}) N_{\text{Xe}}$ (cgs units).

Some aspects of the theory of this paper for the processes $\omega_1 + \omega_1 - \omega_3 \rightarrow \omega_4$ and $\omega_1 + \omega_1 + \omega_3 \rightarrow \omega_4$ have been verified in a series of experiments performed by Kung.⁴ These experiments concerned the mixing of a fixed frequency pump at 2660 Å ($\omega_p = \omega_1$) with a variable frequency signal or idler ($\omega_s, \omega_i = \omega_3$) in Xe gas to produce tunable coherent vacuum ultraviolet radiation. Kung's experimental configuration involved very tight focusing of the fundamental beams. Figure 17 shows the maximum possible spectral range which would be predicted for each process on the basis of simple addition or subtraction of the available fundamental photon energies. Figure 17 also shows the range of tunable VUV output actually observed by Kung. The process $\omega_1 + \omega_1 + \omega_3 \rightarrow \omega_4$ produced a detectable signal at ω_4 only when ω_4 was near to, and on the short wavelength side of a strong Xe line. This is a necessary condition to produce anomalous dispersion and thus the negative values for Δk necessary to optimize G_1 . The process $\omega_1 + \omega_1 - \omega_3 \rightarrow \omega_4$, however, produced a detectable signal over the entire maximum possible spectral range. This result would be expected since G_2 may be optimized for either negative or positive Δk . Thus the theory qualitatively explains the results of these experiments.

TUNABLE VUV

$$\omega_i = 7200\text{\AA} \longrightarrow 5320\text{\AA}$$

$$\omega_s = 5320\text{\AA} \longrightarrow 4200\text{\AA}$$

$$\omega_p = 2660\text{\AA}$$

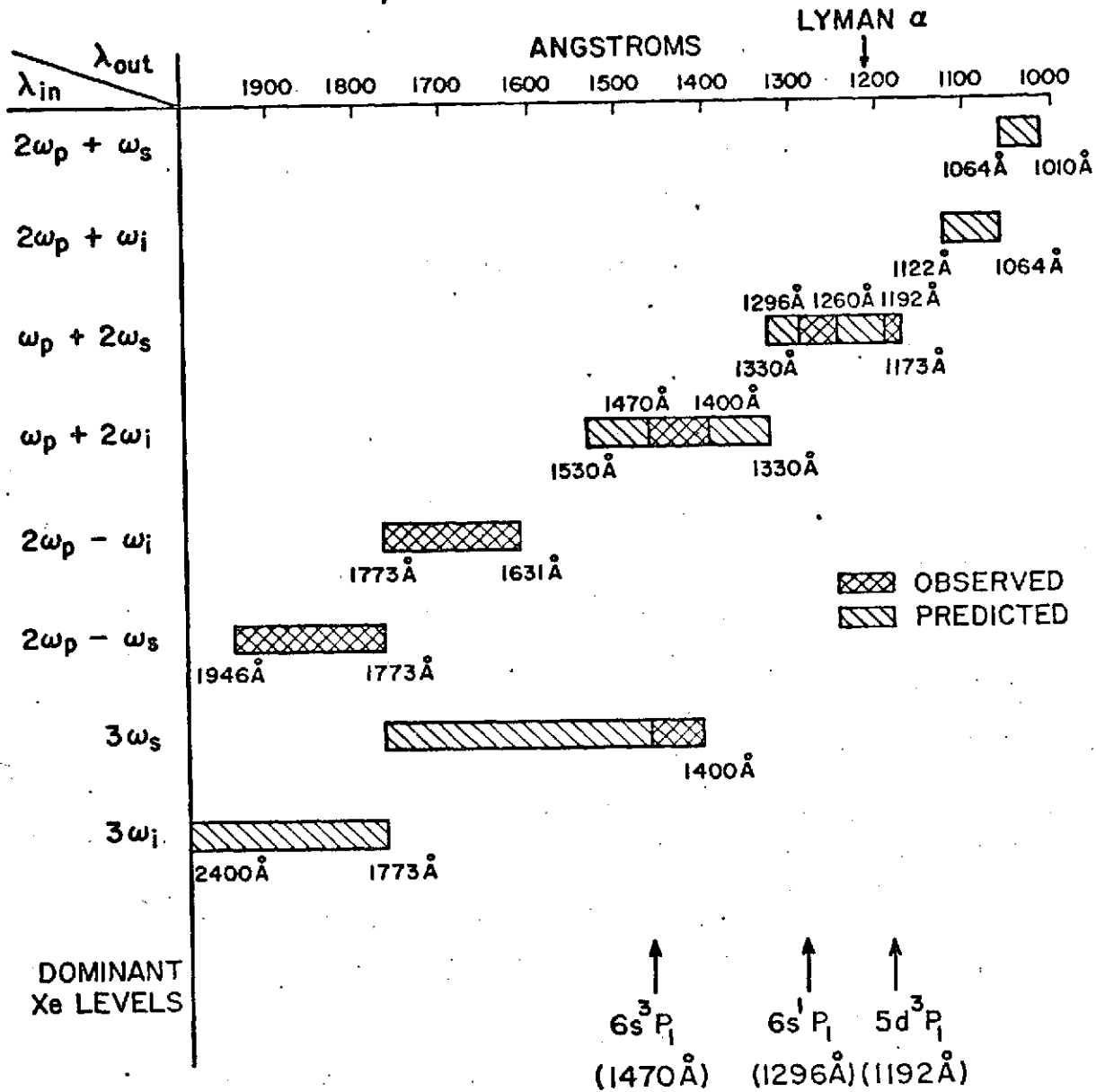


Fig. 17--Summary of the tunable VUV output achieved by Kung. ω_p = pump frequency at 2660 Å, ω_s = signal frequency tunable from 5320 Å to 4200 Å, ω_i = idler frequency tunable from 7200 Å to 5320 Å.

VII. CONCLUSIONS

This paper has presented a theoretical and experimental investigation of the effects of focusing on third-order nonlinear processes in isotropic media. A rigorous theory which relates the total power and far-field beam profile of the generated radiation to the various parameters of the fundamental beams and to the wave vector mismatch has been developed. In the case of tight focusing with the fundamental beam waist region entirely contained within the cell, it has been shown that the process $\omega_1 + \omega_2 + \omega_3 \rightarrow \omega_4$ can be efficient only in media whose dispersion characteristics produce a negative wave vector mismatch and that the process $\omega_1 - \omega_2 - \omega_3 \rightarrow \omega_4$ can be efficient only in media whose dispersion characteristics produce a positive wave vector mismatch. The process $\omega_1 + \omega_2 - \omega_3 \rightarrow \omega_4$ can be efficient in media with all types of dispersion characteristics and is always optimized by focusing as tightly as possible.

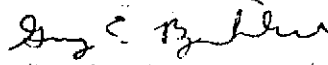
The improved understanding contributed by this paper of the far-field beam profile of the generated radiation for the process $\omega_1 + \omega_2 - \omega_3 \rightarrow \omega_4$ has important applications for coherent anti-Stokes Raman spectroscopy. By controlling the value of $b\Delta k$, the mode of the output radiation may be varied from near Gaussian to a ring shaped pattern of variable cone angle. The cone angle of this ring pattern may be increased to the point where the generated radiation and the Gaussian fundamental beams become completely

spatially separated in the far field. The advantages in detectivity which accrue from spatial separation between the generated radiation and fundamental beams may thus be secured for geometries which involve colinear propagation of the fundamental beams.

In the VUV and soft x-ray spectral regions index of refraction data is often completely lacking and even the sign of the wave vector mismatch produced by various media may be unknown. In this case, if Δk is of the wrong sign and/or if b is of the wrong value, the efficiencies of the processes $\omega_1 + \omega_2 + \omega_3 \rightarrow \omega_4$ and $\omega_1 - \omega_2 - \omega_3 \rightarrow \omega_4$ may be reduced by several orders of magnitude. Thus the process $\omega_1 + \omega_2 - \omega_3 \rightarrow \omega_4$ with very tight focusing has the highest probability of successfully producing a sufficient output for detection.

VIII. ACKNOWLEDGEMENTS

The author is pleased to acknowledge many stimulating and helpful conversations with S. E. Harris, R. L. Byer, D. M. Bloom, A. H. Kung, E. A. Stappaerts, D. W. Phillion, and especially J. F. Young. The author is also indebted to C. M. Bjorklund for help in preparing the figures and to B. Yoshizumi for help in constructing the apparatus.



G. C. Bjorklund

HO-1313-GCB-js

Atts.
References
Figure Captions

REFERENCES

1. R. B. Miles and S. E. Harris, "Optical Third-Harmonic Generation in Alkali Metal Vapors," IEEE J. Quant. Elect. QE-9, 470 (1973).
2. D. M. Bloom, G. W. Bekkers, J. F. Young, and S. E. Harris, "Third Harmonic Generation in Phase Matched Alkali Metal Vapors," Appl. Phys. Letters (submitted for publication).
3. R. T. Hodgson, P. P. Sorokin, and J. J. Wynne, "Tunable Coherent Vacuum-Ultraviolet Generation in Atomic Vapors," Phys. Rev. Letters 32, 343 (1974).
4. A. H. Kung, "Generation of Tunable Picosecond VUV Radiation," Appl. Phys. Letters 25, 653 (1974).
5. A. H. Kung, J. F. Young, G. C. Bjorklund, and S. E. Harris, "Generation of Vacuum Ultraviolet Radiation in Phase-Matched Cd Vapor," Phys. Rev. Letters 29, 985 (1972).
6. A. H. Kung, J. F. Young, and S. E. Harris, "Generation of 1182 Å Radiation in Phase-Matched Mixtures of Inert Gases," Appl. Phys. Letters 22, 301 (1973).
7. S. E. Harris and D. M. Bloom, "Resonantly Two-Photon Pumped Frequency Converter," Appl. Phys. Letters 24, 229 (1974).
8. D. M. Bloom, James T. Yardley, J. F. Young, and S. E. Harris, "Infrared Up-Conversion With Resonantly Two-Photon Pumped Metal Vapors," Appl. Phys. Letters 24, 427 (1974).

9. P. P. Sorokin, J. J. Wynne, and J. R. Lankard, "Tunable Coherent IR Source Based Upon Four-Wave Parametric Conversion in Alkali Metal Vapors," *Appl. Phys. Letters* 22, 342 (1973).
10. P. D. Maker and R. W. Terhune, "Study of Optical Effects Due to an Induced Polarization Third Order in the Electric Field Strength," *Phys. Rev.* 137, 801 (1965).
11. P. R. Regnier and J. P. Taron, "On the Possibility of Measuring Gas Concentrations by Stimulated Anti-Stokes Scattering," *Appl. Phys. Letters* 23, 240 (1973).
12. M. D. Levenson, "Feasability of Measuring the Nonlinear Index of Refraction by Third-Order Frequency Mixing," *IEEE J. Quant. Elect.* QE-10, 110 (1974).
13. R. F. Begley, A. B. Harvey, and R. L. Byer, "Coherent Anti-Stokes Raman Spectroscopy," *Appl. Phys. Letters* 25, 387 (1974).
14. J. F. Ward and G. H. C. New, "Optical Third Harmonic Generation in Gases by a Focused Laser Beam," *Phys. Rev.* 185, 57 (1969).
15. D. A. Kleinman, A. Ashkin, and G. D. Boyd, "Second-Harmonic Generation of Light by Focused Laser Beams," *Phys. Rev.* 145, 338 (1966).
16. G. D. Boyd and J. P. Gordon, "Confocal Multimode Resonator for Millimeter Through Optical Wavelength Masers," *Bell Systems Tech. J.* 40, 489 (1961).
17. D. A. Kleinman, "Theory of Second Harmonic Generation of Light," *Phys. Rev.* 128, 1761 (1962).
18. O. Buneman, private communication.

19. R. W. Terhune, "Nonlinear Optics," *Solid State Design* 4, 38 (1963);
and B. P. Stoicheff, "Characteristics of Stimulated Raman Radiation
Generated by Coherent Light," *Phys. Letters* 7, 186 (1963).

LIST OF FIGURES

1. F_1 vs. $b\Delta k$ for $b/L \leq 0.1$ and $f/L = 0.5$.
2. F_2 vs. $b\Delta k$ for $b/L \leq 0.1$; $f/L = 0.5$; and $k''/k' = 1.0$, 1.1 , 1.5 , 2.0 , and 3.0 .
3. F_3 vs. $b\Delta k$ for $b/L \leq 0.1$; $f/L = 0.5$; and $k''/k' = 1.0$, 1.1 , 1.5 , 2.0 , and 3.0 .
4. F_1 vs. $b\Delta k$ for $f/L = 0.5$ and $b/L = 0$, 0.3 , 0.5 , 0.75 , 1.0 , and 2.0 .
5. F_1 vs. $b\Delta k$ for $f/L = 0.5$ and $b/L = 0$, 1 , 2 , and 3 .
6. F_1 vs. $b\Delta k$ for $b/L = 0.1$ and $f/L = 0.5$, 0.75 , 0.85 , 1.0 , and 1.5 .
7. F_1 vs. $b\Delta k$ for $b/L = 0.3$ and $f/L = 0.5$, 0.75 , 1.0 , and 1.5 .
8. F_1 vs. $b\Delta k$ for $b/L = 1$ and $f/L = 0.5$, 0.75 , 1.0 , and 1.5 .
9. F_1 vs. $b\Delta k$ for $b/L = 3$ and $f/L = 0.5$, 0.75 , 1.0 , 1.5 , and 5.0 .
10. F_1 vs. $b\Delta k$ for $b/L = 10$ and $f/L = 0.5$, 1.0 , 1.5 , and 2.0 .
11. Far-field intensity distribution for several values of $b\Delta k$ for the process $\omega_1 + \omega_2 - \omega_3 \rightarrow \omega_4$ with $k''/k' = 3.0$. The distribution in each case is calculated at the position of the output window of a cell with $b/L = 0.1$ and $f/L = 0.5$.
12. G_1 vs. $b\Delta k$ for $b/L \leq 0.1$ and $f/L = 0.5$, 0.75 , and 0.85 .

13. G_2 vs. $b\Delta k$ for $b/L \leq 0.1$; $f/L = 0.5$; and $k''/k' = 1.0$, 1.5 , and 3.0 .
14. G_2 vs. $b\Delta k$ for $b/L \leq 0.1$; $f/L = 0.5$; and $k''/k' = 1.1$ and 2.0 .
15. G_3 vs. $b\Delta k$ for $b/L \leq 0.1$; $f/L = 0.5$; and $k''/k' = 1.0$, 1.1 , 1.5 , 2.0 , and 3.0 .
16. Relative power output at 1182 \AA vs. Xe pressure. (The triangular points represent data from a run in which the shearing aperture was set to the proper diameter. The circular points represent data from a run in which the shearing aperture was open too far. The solid curve represents the best fit to the function $G_1(b\Delta k, 0, 0.5, 1)$ to the triangular points.)
17. Summary of the tunable VUV output achieved by Kung. ω_p = pump frequency at 2660 \AA , ω_s = signal frequency tunable from 5320 \AA to 4200 \AA , ω_i = idler frequency tunable from 7200 \AA to 5320 \AA .